

# Molecular docking, dynamic simulations, and network pharmacology approach to explore the therapeutic potential of *Zanthoxylum armatum* phytochemicals against Malaria

Khan Hamna <sup>1</sup>, Bibi Ayesha <sup>1</sup>, Amber Sanila <sup>1</sup>, Mukhtar Mamuna <sup>2</sup>, Ahmad Nouman <sup>1</sup>, Khan Haris Ahmed <sup>1</sup>

<sup>1</sup> Department of Biotechnology, University of Mianwali, Mianwali, Punjab 42200, Pakistan.

<sup>2</sup> Atta-ur-Rahman School of Applied Biosciences, National University of Sciences and Technology (NUST), H-12. 44000 Islamabad, Pakistan.

♦Corresponding author: [hakhan@umw.edu.pk](mailto:hakhan@umw.edu.pk)

**Subject Area:**  
Biomedical Sciences

Received: May 02, 2025  
Accepted: July 10, 2025  
Published: July 24, 2025

**Citation:** Khan H, Bibi A, Amber S, Mukhtar M, Ahmad N, and Khan HA. 2025. Molecular docking, dynamic simulations, and network pharmacology approach to explore the therapeutic potential of *Zanthoxylum armatum* phytochemicals against Malaria. Bioc Scientia 1(2). <https://doi.org/10.63622/RBS.2507>



**Copyright:** © 2024 by the authors. Submitted for possible open access publication under the terms and conditions of the Creative Commons Attribution (CC BY-NC) license (<https://creativecommons.org/licenses/by/4.0/>).

**Abstract:** Malaria continues to be a global health challenge mainly due to drug resistance that necessitates the innovative approaches in pharmaceutical development. Therefore, in the present study, we investigated the therapeutic potential of natural plant-based phytochemicals from *Zanthoxylum armatum* against malaria. Based on pharmacokinetic and ADMET properties analysis, a total of 40 compounds were identified, and these were analyzed and screened in accordance with Lipinski rule of five. The Molecular docking, dynamic simulations, and network pharmacology approach was used to validate the role of selected phytochemicals against malarial target proteins such as PfAMA-1, Pf GST, and PfDHFR. Molecular docking experiments revealed the strong interactions of the three phytochemicals: Cuminal, Sabinene, and Phellandral with the key malarial targets. Molecular dynamic (MD) simulations further confirmed the stability and flexibility of these docked complexes. Furthermore, the network pharmacology analysis identified 23 common targets of these three active phytochemicals and malaria, some of these protein targets include ALB, CXCL8, NOS2, HMOX1, MPO, TNF, IL6, and PTPRC. These proteins are mainly involved in inflammatory response and oxidative stress, the key mechanisms involved in malarial infection, so regulating these targets may prove beneficial in treating *Plasmodium falciparum*-induced malaria. These findings provide strong basis for further *in-vitro* and *in-vivo* studies to validate the role of Cuminal, Sabinene, and Phellandral as substantial drug candidates against malaria.

**Keywords:** Malaria, *Zanthoxylum armatum*, *Plasmodium falciparum*, Molecular docking, MD simulations, Network pharmacology.

**Resumen:** La malaria sigue siendo un desafío de salud global principalmente debido al aumento de la resistencia a los medicamentos existentes, lo que resalta la necesidad de enfoques innovadores en el desarrollo de fármacos. Por lo tanto, el presente estudio investiga el potencial terapéutico de los fitoquímicos de origen vegetal de *Zanthoxylum armatum* como agentes antipalúdicos. Basado en el análisis de propiedades farmacocinéticas y ADMET, se identificaron y evaluaron un total de 40 compuestos de acuerdo con la regla de cinco de Lipinski. Se utilizó el acoplamiento molecular, las simulaciones dinámicas y el enfoque de farmacología de red para validar el papel de los fitoquímicos seleccionados contra proteínas diana del paludismo como PfAMA-1, Pf GST y PfDHFR. Los experimentos de acoplamiento molecular revelaron las fuertes interacciones de los tres fitoquímicos; Cuminal, sabineno y phelantral con los objetivos clave de la malaria. Las simulaciones de dinámica molecular (MD) confirmaron además la estabilidad y flexibilidad de estos complejos acoplados. Además, el análisis de farmacología de redes identificó 23 objetivos comunes de estos tres fitocompuestos activos y la malaria, algunos de estos objetivos proteicos incluyen ALB, CXCL8, NOS2, HMOX1, MPO, TNF, IL6 y PTPRC. Estas proteínas están principalmente involucradas en la respuesta inflamatoria y el estrés oxidativo, los mecanismos clave involucrados en la infección por malaria, por lo que regular estos objetivos puede resultar beneficioso en el tratamiento de la malaria inducida por *Plasmodium falciparum*. Estos hallazgos proporcionan una base sólida para estudios adicionales *in vitro* e *in vivo* que validen el papel del Cuminal, sabineno y phelantral como candidatos a fármacos sustanciales contra la malaria.

**Palabras clave:** Malaria, *Zanthoxylum armatum*, *Plasmodium falciparum*, Acoplamiento molecular, Simulación de dinámica molecular, Farmacología de red.

## INTRODUCTION

Malaria affects 219 million people worldwide, leading to 435,000 deaths annually (Citaristi, 2022). The highest number of malarial cases has been reported in Africa and certain Asian countries and the prevalence of the disease is increasing since 2015 (PAH, 2017a; PAH, 2017b; Basu and Sahi, 2017). *Plasmodium*, the causative agent of malaria, affects humans and accumulates malarial pigment in the form of an insoluble haemoglobin metabolite (Miller *et al.*, 1994; Phillips y Pasvol, 1992). These parasites can be found in various vertebrates, including red blood cells and human tissues. The deadliest and highly pathogenic form of *Plasmodium* is known as *Plasmodium falciparum* which causes malaria in humans (Prugnolle *et al.*, 2011; Daxon, 2019; Ogony, 2021). The main symptoms include chills, fever, and headaches and these symptoms arise primarily due to the destruction of erythrocytes (Tahita *et al.*, 2013; Greenwood, 2019; Fikadu and Ashenafi, 2023).

The mortality rate due to malaria has decreased due to the increased antimalarial drugs that is now safe, efficient, and cost-effective (Warrel *et al.*, 2017). Drugs mainly include quinine, chloroquine, pyrimethamine, sulfonamides, sulfones, and artemisinin derivatives. Two of the commonly used drugs artesunate and sulfadoxine mainly perform their antimalarial action via inhibiting protozoal glutathione S-transferase (GST) and dihydrofolate reductase (DHFR). However, the malaria parasite rapidly modifies itself, thus causing antimicrobial resistance and difficulties in the development of efficient vaccines and drugs (Narwal *et al.*, 2024). Therefore, scientists are striving hard to develop alternative, safer and more cost-effective treatment options against malaria.

Plant-based compounds such as flavonoids, terpenoids, alkaloids, tannins, steroids, resins, phenolic compounds, and other metabolites are frequently used in research related to drug development due to their antimicrobial, antioxidant, anti-inflammatory, antiviral, and anticancer properties (Guadie *et al.*, 2020; Malami *et al.*, 2022). *Zanthoxylum armatum* DC., also known as Indian prickly ash or Nepal pepper, belongs to the Rutaceae family (Sharma *et al.*, 2021). The species typically inhabits valleys and thickets mountains, wastelands, and forests. In traditional systems of medical treatment, *Z. armatum* tree bark, fruits, and seeds were widely used as carminatives, stomach, and anthelmintics, and the dried fruit served as a spice (Barkatullah *et al.*, 2014). Fruit and seeds were also used to treat dyspepsia and fever with an aromatic tonic useful for dental problems, and their ointment is used to treat infestations (Iqbal and Hamayun, 2004). The extract of *Z. armatum* has effective anti-skin sensitivity, loculicidal, anti-inflammatory, antibacterial, antifungal, and cytotoxic activities (Peana *et al.*, 2002; Khan *et al.*, 2008).

Therefore, the present study has been conducted to assess the inhibitory capabilities of 40 phytochemicals that include terpenoids, flavonoids, alkaloids, carbonyls, and coumarins, all sourced from *Z. armatum*. Three proteins / antigens were selected as a target against compounds based on *Z. armatum* and these include *P.*

*falciparum* glutathione S-transferase (Pf GST), *P. falciparum* dihydrofolate reductase (PfDHFR), and *P. falciparum* apical membrane antigen 1 (PfAMA-1). Pf GST acts as a peroxidase, and it is mainly overexpressed in chloroquine resistance strains. Therefore, it can act as a potential target for drugs that can be used in combination with chloroquine to effectively treat malaria. PfDHFR is mainly responsible for DNA and folate synthesis and various other metabolic pathways in the malarial parasite therefore, its inhibition may lead to suppression of the growth of plasmodium (Shamshad et al., 2022). Furthermore, PfAMA-1 is a type 1 integral membrane protein that consists of 3 domains and is involved in the entry of the parasite into the hepatocytes of the host to evoke the immune response (Obonyo, 2022). Therefore, its binding to cell surface receptors can be inhibited to prevent the entry of this pathogenic antigen inside cells.

In the present study, a pharmacokinetic analysis was performed to assess the drug-like properties and toxic potential of these phytochemicals. Molecular docking was carried out to identify the interactions between these compounds and target proteins from *P. falciparum* involved in the pathogenesis of malaria. The stability of the docked complexes was confirmed through molecular dynamic simulations and the network pharmacology approach was used to further anticipate the toxicity, classification, and bioactivity of the selected phytochemicals.

## MATERIALS AND METHODS

### Selection of Ligands and Receptors (accessed in April 2024)

The molecular structures of the 40 *Z. armatum*-based compounds (Ahmad, Misra and Gupta, 1993; Tiwary et al., 2007; Dhami et al., 2018) and 2 commonly used antimalarial drugs sulfadoxine (Francis et al., 2020) and artesunate (Khanal, 2021) were obtained from PubChem in SDF format and converted to PDB files using Biovia Discovery Studio v2021 software (ter Kuile et al., 2007; Phuyal et al., 2019). The necessary charges like water molecules that were removed and hydrogen atoms were added were incorporated to prepare the ligands and then saved in PDBQT format for additional analysis and computational assessments. The names, molecular weight, formulas, Pubchem IDs, and structures of the selected ligands are provided in the Supplementary Table 1. Three of the proteins were selected as targets against the 40 *Z. armatum*-based compounds, including Pf GST (PDB ID: 1OKT), Pf DHFR (PDB ID: 7F3Y), and Pf AMA-1 (PDB ID: 1Z40) and their 3D structures were obtained from RCSB PDB.

Subsequently, using Discovery Studio software for protein 3D structure refinements, the ligands and other small molecules or atoms were eliminated from the receptors. Further refinements were made by removing water molecules, adding polar hydrogen atoms, and assigning charges. The final refined receptor structure was saved in PDBQT format, for docking experiments (Figure 1). The canonical SMILES (Simplified Molecular Input Line Entry System) notations for each compound were retrieved from the PubChem database (<https://pubchem.ncbi.nlm.nih.gov>).

### Prediction of Activity Spectra for Substances (PASS) Analysis

The Prediction of Activity Spectra for Substances (PASS) analysis program (accessed in April 2025) was used to predict the biological properties, pharmacological characteristics, drug-likeness, potential side effects, and possible mode of action of the selected constituents. These predictions are made based on the structural and active relationships observed with established chemical entities (Khan et al., 2017). PASS Online (<http://www.pharmaexpert.ru/passonline/>), which offers probability of activity (Pa) and inactivity (Pi) for a broad range of pharmacological effects, was used to forecast the possible biological activities of a few chosen phytochemicals. Activities were only deemed noteworthy if their Pa was more than 0.7. Lipinski's Rule of Five, Veber's Rule, and pharmacokinetic properties such as gastrointestinal absorption, blood-brain barrier permeability, P-glycoprotein substrate/inhibitor status, and CYP inhibition profile were assessed using SwissADME (<http://www.swissadme.ch/>) (accessed in June 2024). ADMET-related metrics and toxicity evaluations were further analyzed through ProTox-II ([https://tox-new.charite.de/protox\\_II](https://tox-new.charite.de/protox_II)) (accessed in July 2024), respectively. Each of these tools was chosen for its ability to accurately predict certain parameters that PASS alone does not offer.

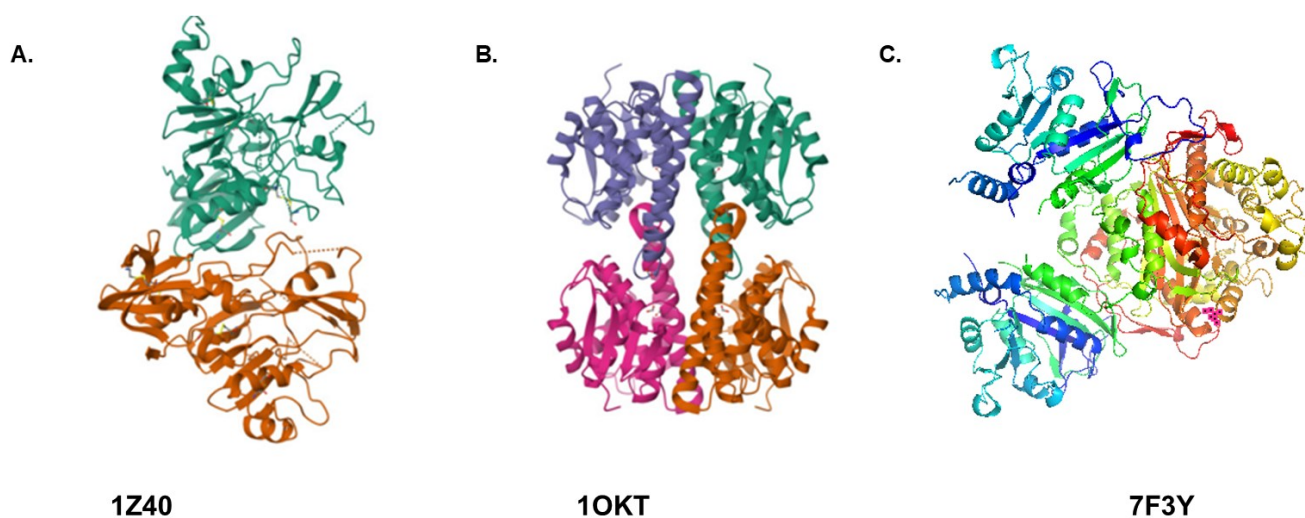


**Figure 1.** Representation of the 3-Dimensional structure of Malarial receptor proteins at the cell surface. **A.** *Pf* Anti-Malarial Antigen1 (*Pf* AMA-1), **B.** *Pf* Glutathione S-Transferase (*Pf* GST), **C.** *Pf* dihydrofolate reductase-thymidylate synthase (*Pf* DHFR-TS).

### Lipinski's Rule of Five (Drug Likeness Analysis)

The pharmacokinetic properties of the selected compounds such as absorption, distribution, excretion, and metabolism were evaluated using Lipinski's rule of five using Molinspirationv2021, (<https://www.molinspiration.com/cgi-bin/properties>) (accessed on May 2024). The determination of Lipinski's rule of five was based on certain predefined criteria, including the logarithm of the partition coefficient between *n*-octanol and water ( $\log P \leq 5$ ), molecular weight ( $MW \leq 500$ ), the number

of hydrogen bond donors ( $\text{NOHNH} \leq 5$ ), hydrogen bond acceptor sites ( $\text{NON} \leq 10$ ), topological polar surface area ( $\text{TPSA} \leq 140 \text{ \AA}^2$ ), and the number of rotatable bonds ( $\leq 10$ ). It is important to note that, to maintain bioavailability, an orally active drug should not exceed a single Lipinski violation (Pollastri, 2010). Drug likeness was also evaluated based on the rules of Ghoshe, Veber, Egen, and Muegge (Arunkumar et al., 2018). The drug-like potential of a compound is the assessment of oral bioavailability and ADMET properties (Kumari et al., 2019). According to Muegge's rule, certain ranges of H-bond donors and acceptors can be used to suggest drug-like effects, the Egen rule is a method for predicting oral bioavailability using molecular polar surface area ( $\text{PSA} \times 131 \times 2$ ) and  $\text{Log P} \times 5.88$ , the Ghosh's rule-based approach that emphasizes on molecular weight ( $\text{MW} < 480$ ),  $\text{Log P}$  (1-3), and atom count (20-70) and in Veber's Rule, 10 rotatable bonds and 140 polar surface areas (PSA) are recommended to maximize oral bioavailability (Ndombera et al., 2019). Additional filters were employed to improve prediction accuracy. Veber's Rule highlights the significance of molecular flexibility and polarity, suggesting a maximum of 10 rotatable bonds and a polar surface area (PSA) of no more than  $140 \text{ \AA}^2$ . Ghose's Rule highlights ideal physicochemical characteristics, indicating a molecular weight range of 160–480 Da,  $\text{LogP}$  from -0.4 to 5.6, molar refractivity between 40 and 130, and a total atom count between 20 and 70. Egan's filter employs  $\text{PSA} \leq 131 \text{ \AA}^2$  and  $\text{LogP} \leq 5.88$  to anticipate membrane permeability. Muegge's Rule combines several parameters such as MW (200–600),  $\text{LogP}$  (-2 to 5), H-bond donors ( $\leq 5$ ), H-bond acceptors ( $\leq 10$ ), and rotatable bonds ( $\leq 15$ ) to recognize drug-like entities. Through the incorporation of these guidelines, compounds were evaluated to confirm advantageous pharmacokinetic properties and a high likelihood of success as orally active therapeutics.

### Bioactivity Score Prediction

The bioactivity score indicates the likelihood that the studied complex could act as a potential drug (accessed on June 2024). The bioactivity score of phytochemicals against malarial target proteins was determined by a computational tool called Molinspiration version 2021.13. The structures were prepared through different options, and their physiochemical features and pharmacokinetic descriptors were calculated. The software indicates these 3 parameters; active, moderately active and inactive that if the score is higher than 0.0, the compound is active; if it is between -0.5 and 0.0, it is moderately active; and if it is less than -0.5, it is inactive (Jindal and Rani, 2023).

### Toxicity Risk Assessment

The study provides an assessment of the anticipated adverse effects of a pharmaceutical compound on human health (Barile, 1996). The Protox-II server was used to evaluate the toxicological properties of phytochemicals found in *Z. armatum*, including aspects such as hepatotoxicity, cytotoxicity, carcinogenicity, mutagenicity, and tumorigenicity. Toxicity categorizations were established in align-



ment with the criteria of the Global Harmonized System (GHS) criteria for the classification and labelling of chemical compounds. The LD50 classes of the active compounds were also evaluated. The LD50 value is the dose of a drug or bioactive compound that kills 50% of the test substances (Banerjee et al., 2018).

### Pharmacokinetic Activity Prediction

Using the online tool Swiss-ADME, predictive modelling was employed to assess the absorption, distribution, metabolism, excretion, and toxicity (ADMET) of all phytochemical compounds and antimalarial drugs under investigation. The ADMET analysis focusses on blood-brain barrier (BBB) permeability, tissue distribution, gastrointestinal absorption, P-glycoprotein (P-gp) substrate, metabolic effects as an inhibitor of CYP3A4, and fluidity pertinent to plasma membrane absorption (Muhammed et al., 2021). PKCSM was used to evaluate the properties of pharmacokinetics ([https://biosig.lab.uq.edu.au/pkcsm/prediction\\_single/](https://biosig.lab.uq.edu.au/pkcsm/prediction_single/)).

### Molecular Docking (accessed in August 2024)

The ligands were docked with receptors using AutoDock version 1.5.6. (Huey et al., 2012). AutoDock vina was used to automatically calculate the grid values. In this research, the Grid box size was 40×40×40 (x, y and the z) and spacing was 0.375 for 3 receptors. Docking was performed using the Lamarckian Genetic Algorithm with an exhaustiveness value of 8 and a maximum of 9 binding modes. The energy range was set to 4 kcal/mol, and the number of evaluations was adjusted to the default settings of AutoDock Vina. For PfAMA-1 (PDB ID:1Z40), the center of the grid box was set at the position 11.657, 12.407, and 63.734 for x, y, and z, respectively. For PfGST (PDB ID: 1OKT) the center was set at the position 50.718, 42.107, and -8.602 for the x, y and z axes, respectively. For PfDHFR (PDB ID: 7F3Y) the grid center was set at 1.265, -1.860, and -23.712 for x, y, and z, respectively. The configuration file containing Grid box values for each ligand was obtained and saved in txt. format. The output was obtained by generating a command or code and saved in PDBQT format. The results showed the binding affinity of ligand to the receptor that was Gibbs free energy in kcal mol<sup>-1</sup>. The highest negative value was considered as the highest binding affinity for receptor proteins. For the above 50 values, the best fit was selected. All profiles were displayed in Discovery Studio and a 2D output image showing the interaction of the ligand with the receptor's amino acids was obtained (Vong et al., 2022).

### Molecular Dynamic Simulations (accessed in June 2025)

Molecular dynamic simulations were performed to study the interactions and movements of docked complexes using the accelerated central processing unit (CPU) platform via GROMACS software (van der Spoel et al., 2005). The system was prepared by charm 36-jul 2022. ff. The docked complexes were separated using Chimera into protein and ligand. For proteins, the additional dock prep with library was done by Dunbrack 2010 rotamers, and for PfDHFR-TS and PfGST protein complexes, the Richardson rotamer library was used. For the analysis of the

PfAMA-1 protein and the prepared ligand, GROMACS files were used from the Swiss Institute of Bioinformatics web server were used (Zoete et al., 2011). The resulting input files were downloaded as GROMACS files. The initial position of the particle was assigned using GROMACS '.gro' files, while the topologies were added in interactions between particles. Long range electrostatic interactions were implemented using particle mesh Ewald method, with cutoff distance of 1.2 nm for van der Waals interactions. The equilibrium was continued in an isothermal-isobaric ensemble maintaining a temperature of 300K for a 100 ns duration. The simulations were executed in the MD integrator with a 2fs time step. For trajectory analysis, MD analysis packages were used to compute the root mean square fluctuation (RMSF), radius of gyration (Rg), and root mean square deviation (RMSD) of both the protein and protein-ligand complexes. These parameters showed deviations and stability of the protein and ligand complexes in the simulation. These dynamics were conducted in GROMACS.

### **Network Pharmacology Approach (accessed in September 2024)**

#### *Screening of the Potential Targets of Selected Compounds*

The data of potential targets of active compounds were retrieved from Swiss Target Prediction (<http://www.swisstargetprediction.ch/>) by entering the canonical SMILES and specifying the species as homo sapiens. However, malarial targets were downloaded from GeneCard (<http://www.genecards.org/>) and DesGenet (<http://www.disgenet.org/>). The targets of these databases were merged, and repetitions were removed. The common names of the targets were also searched from UniProtKB (<https://www.uniprot.org/>). The mutual targets of the selected compounds and the malaria were achieved, and Venn diagram was constructed using the bioinformatics tool (<https://bioinformatics.psb.ugent.be/webtools/Venn>) (Tabassum et al., 2022).

#### *Construction of Compound Target Network*

Cytoscape V3.10.1 was used (<https://cytoscape.org/>) to build the compound-targets network to study the interactions among active compounds within the intricate biological system. In this network, the nodes represent the chemical constituents and targets, while the edges represent their interactions. The network analyzer function was employed to assess the basic characteristics of the network. Subsequently, the network was filtered based on the "degree," which indicates the number of connected nodes linked to a specific network node as a node attribute (Ram et al., 2023).

#### *Prediction of Protein–Protein Interaction Network and Hub Genes*

The STRING database (<https://stringdb.org/>) was used to evaluate the protein-protein interaction of 340 common genes, with the organism specified as "*Homo*

*sapiens*". Cytoscape V3.10.1 was utilized to visualize the protein-protein interaction network. Identification of hub genes and nodes with elevated degrees within the network was carried out using the CytoHubba plugin (Tao et al., 2013).

### *Construction of target–compound–pathway network*

The DAVID database (<https://david.ncifcrf.gov/tools.jsp>) provided the data for the analysis of the top hub genes, and a network was created to examine the mechanism within these pathways (Tabassum et al., 2022).

### *Gene Ontology and KEGG Pathway Analysis*

The DAVID functional gene annotation resource database (<http://david.ncifcrf.gov/>) was used to conduct Gene Ontology and KEGG pathway analyses for the "*Homo sapiens*". It categorized gene functions into biological processes (BP), cellular components (CC), and molecular functions (MF) using Gene Ontology analysis, as well as performing enrichment pathway analysis for KEGG pathways. To visualize the results, top 20 GO annotations (BP, CC, and the MF) and KEGG pathways were selected using a cutoff method with a probability score below  $5 \times 10^{-2}$ . The bars and lollipop plots were created using Shiny GO (<http://bioinformatics.sdstate.edu/go/>) for the selected annotations and pathways (Pomaznoy et al., 2018).

## **RESULTS**

### **Lipinski's Rule of Five (Drug Likeness Analysis)**

This analysis provided the phytochemical properties of 40 phytoconstituents of *Z. armatum* (Shah et al., 2024). Tambuletin exhibited more than 3 violations while Lupeol,  $\alpha$ -Amyrins, Nerol, *allo*-Aromadenderene, (*E*)-Nerolidol and  $\beta$ -caryophyllene showed 1 violation. The remaining compounds did not show any violations of Lipinski's rule (Supplementary Table 2). An ideal compound should not contain more than one violation. The results of the Ghoshe, Veber, Egen, and Muegge rules are provided in the (Supplementary Table 3).

### **Bioactivity Score Prediction**

Prediction of the bioactivity score showed that the score is higher than 0.0, the compound is active; if it is between -0.5 and 0.0, it is moderately active; and if it is less than -0.5, it is inactive. Cuminal (-0.44), Sabinene (-0.33), and Phellandral (-0.04) are important moderately active ion channel modulators, while Phellandral also revealed the potential to act as inactive nuclear receptor ligand (-1.50) and a moderately active enzyme inhibitor (-0.27). Lupeol is an active GCPR ligand (0.27), nuclear receptor inhibitor (0.85), protease inhibitor (0.15), and enzyme inhibitor (0.52) but is moderately active as a kinase inhibitor (-0.42).  $\alpha$ -Amyrins and Tambuletin are active GCPR ligands (0.22, 0.10), nuclear (0.79, 0.16), protease



(0.19, 0.24), and enzyme inhibitors (0.60, 0.36), but moderately active ion channel modulators (-0.02, -0.04) and kinase inhibitors (-0.41, -0.18). The  $\alpha$ -Terpinene is an active ion channel modulator (0.24), nuclear receptor inhibitor (0.24), protease inhibitor (0.52), enzyme inhibitor (0.11) and kinase inhibitor (0.29) but an inactive GCPR ligand (-0.96). Pyrimethamine and sulfadoxine are inactive nuclear-receptor ligands (-0.62). Details of all other phytochemicals are presented in (Table 1).

**Table 1.** Bioactivity Score prediction of phytochemicals of *Z. armatum*.

Phytoconstituents	GPCR ligand	Ion channel modulator	Kinase inhibitor	Nuclear receptor ligand	Protease inhibitor	Enzyme Inhibitor
$\alpha$ -Fenchol	-0.56	-0.46	-1.71	-0.80	-0.67	-0.59
$\alpha$ -Terpinene	-0.96	0.24	0.29	0.24	0.52	0.11
$\alpha$ -Thujene	-0.86	-0.37	-1.73	-0.86	-0.82	-0.48
$\alpha$ -Thujone	-0.75	-0.50	-1.63	-1.08	-0.64	-0.53
$\alpha$ -pinene	-0.48	-0.43	-1.50	-0.62	-0.85	-0.34
$\alpha$ -Terpineol	-0.51	0.15	-1.45	-0.02	-0.78	0.14
$\beta$ -Terpineol	-0.63	0.23	-1.60	-0.21	-0.92	-0.07
Camphor	-0.79	-0.56	-2.12	-1.21	-0.95	-0.52
Citral	-0.86	-0.25	-0.29	-0.42	-0.57	0.02
Citronellol	-0.81	-0.24	-1.16	-0.61	-0.83	-0.12
Citronellal	-0.83	-0.08	-1.30	-0.61	-0.50	-0.03
1'8-cineole	-0.93	0.01	-1.60	-1.07	-0.90	-0.15
Geraniol	-0.60	0.07	-1.32	-0.20	-1.03	0.28
$\gamma$ -terpinene	-0.90	-0.24	-1.37	-0.33	-1.55	-0.07
Limonene	-0.91	-0.27	-2.01	-0.34	-1.38	-0.21
Linalool	-0.73	0.07	-1.26	-0.06	-0.94	0.07
Nerol	-0.60	0.07	-1.32	-0.20	-1.03	0.28
P-cymene	-1.18	-0.61	-1.40	-1.21	-1.42	-0.78
Piperitone	-0.99	-0.60	-2.12	-0.57	-0.96	-0.08
Sabinene	-1.15	-0.33	-1.79	-0.69	-0.78	-0.60
Tagetonol	-0.76	-0.13	-1.75	-0.28	-0.47	0.01
Terpinen-4-ol	-0.56	-0.04	-1.68	-0.20	-0.92	0.06
(Z)-linalool oxide	-0.67	-0.31	-0.95	-0.34	-0.93	0.12
allo-Aromadendrene	-0.67	-0.47	-0.98	-0.21	-0.67	-0.30
(E)-nerolidol	-0.17	0.21	-0.64	0.42	-0.43	0.39
$\alpha$ -Amyrins	0.22	-0.02	-0.41	0.79	0.19	0.60
lupeol	0.27	0.11	-0.42	0.85	0.15	0.52
Cis-ocimene	-0.98	-0.08	-1.26	-0.49	-1.24	0.06
Cuminal	-1.15	-0.44	-1.22	-0.86	-1.48	-0.64
Cinamaldehyde	-1.15	-0.44	-1.22	-0.86	-1.48	-0.64
Phellandral	-0.77	-0.07	-1.50	-0.36	-0.97	-0.27
2-tridecanone	-0.54	-0.18	-1.02	-0.41	-0.56	-0.07
Umbelliferon	-1.22	-0.72	-1.30	-0.92	-1.30	-0.35
Bergapten	-0.16	-0.20	-0.45	-0.03	-0.28	-0.35
3,5-diacetylTambulin	-0.21	-0.15	-0.16	-0.09	-0.32	0.14
Kaempferol	-0.10	-0.21	0.21	0.32	-0.27	0.26
Tambulin	-0.18	-0.16	0.11	0.10	-0.27	0.17
Tambuletin	0.10	-0.04	-0.18	0.16	0.24	0.36
Artesunate	0.08	0.04	-0.20	0.35	0.15	0.31
Sulfadoxine	0.26	-0.21	0.16	-0.62	-0.18	0.10

## Pharmacokinetic Properties

The pharmacokinetic assessment of potential compounds includes essential factors that evaluate their performance in the human body. Gastrointestinal (GI) absorption signifies the likelihood of oral bioavailability, and strong GI absorption enhances the effectiveness of oral delivery. Blood-brain barrier (BBB) permeability indicates a compound's capacity to reach the central nervous system, which is vital for medications aimed at neurological disorders. The classification of a compound as a P-glycoprotein (P-gp) substrate dictates whether it can be expelled from cells, which may influence its absorption and distribution. Furthermore, the inhibition of cytochrome enzymes specifically CYP1A2, CYP2C19, CYP2C9, CYP2D6, and CYP3A4 can affect the metabolism of other medications, raising potential concerns regarding drug-drug interactions and toxicity. The skin permeability coefficient (Log Kp) also sheds light on the likelihood of transdermal absorption, with more negative values signifying reduced permeability. Collectively, these factors offer a thorough insight into a compound's ADME (Absorption, Distribution, Metabolism, and Excretion) profile, critical for evaluating its drug-likeness and therapeutic potential.

The results revealed that  $\beta$ -caryophyllene 0.733, Lupeol 0.72, Tambulin, Tambuletin 0.7, Kaempferol 0.7, and 3,5-Diacetyltumbulin 0.7 were unable to cross the blood-brain barrier (BBB), while the remaining phytochemicals showed permeability to the BBB. Tambuletin showed positive responses against P-gp substrate and the remaining compounds exhibited negative results. Most of the substances were expected to inhibit the various classes of cytochromes (CYP450, CYP1A2, CYP2C19, CYP2C9, CYP2D6, and CYP3A4) for continuous plasma concentrations and increased bioavailability (Table 2). Among these results Tambuletin show positive response to p-gp substrate and show only favorable BBB permeability but lack p-gp substrate activity, making them strong candidate for further *in vivo* evaluation.

## Toxicity Assessment Analysis

Using the Protox-II server the drug-likeness and toxicity potential of different ligands were estimated. The criteria for parameters are; High risk values is any probability > 0.8 in mutagenicity, hepatotoxicity, immunotoxicity, cytotoxicity, or carcinogenicity and LD50 < 300 mg/kg (Class I–III). Moderately risk probability includes 0.6-0.8 and LD50 between 300-200mg/kg (Class IV). Low risk includes <0.6 and LD >2000mg/kg (Class V–VI). 10 compounds;  $\alpha$ -Fenchol (0.96),  $\alpha$ -Terpineol (0.96), (Z)-Linalool oxide (0.96), *allo*-Aromadendrene (0.96),  $\beta$ -Caryophyllene (0.96),  $\alpha$ -Amyrins (0.98), 3,5-Diacetyltambuletin (0.90), Tambulin (0.98) and Tambuletin (0.87) were proven highly immunotoxic and Lupeol (0.57) was slightly immunotoxic. (Z)-linalool oxide (0.69), *allo*-Aromadendrene (0.69),  $\beta$ -Caryophyllene (0.69) were slightly hepatotoxic and Cinnamic aldehyde (0.72) and Bergapten (0.75) were mutagenic. Tambuletin was slightly cytotoxic (0.50) while Bergapten (0.84) showed carcinogenic properties and Umbelliferon (0.64) and P-

Cymene (0.64) were also slightly carcinogenic. Sulfadoxine was also slightly carcinogenic (0.52) (Table 3).

**Table 2.** Pharmacokinetics properties of phytochemicals of *Z. armatum*

Phytoconstituents	GI absorption	BBB permeant	P-gp substrate	CYP1A2 inhibitor	CYP2C19 inhibitor	CYP2C9 inhibitor	CYP2D6 inhibitor	CYP3A4 inhibitor	Log Kp
<b><math>\alpha</math>-Fenchol</b>	High	Yes	No	No	No	No	No	No	-4.99 cm/s
<b><math>\alpha</math>-Terpinene</b>	Low	Yes	No	No	No	No	No	No	-4.11 cm/s
<b><math>\alpha</math>-Thujene</b>	Low	Yes	No	No	No	No	No	No	-5.11 cm/s
<b><math>\alpha</math>-Thujone</b>	High	Yes	No	No	No	No	No	No	-5.62 cm/s
<b><math>\alpha</math>-pinene</b>	Low	Yes	No	No	No	Yes	No	No	-3.95 cm/s
<b><math>\alpha</math>-Terpineol</b>	High	Yes	No	No	No	No	No	No	-4.83 cm/s
<b><math>\beta</math>-Terpineol</b>	High	Yes	No	No	No	No	No	No	-5.45 cm/s
<b>Camphor</b>	High	Yes	No	No	No	No	No	No	-5.67 cm/s
<b>Citral</b>	High	Yes	No	No	No	No	No	No	-5.08 cm/s
<b>Citronellol</b>	High	Yes	No	No	No	No	No	No	-4.52 cm/s
<b>Citronellal</b>	High	Yes	No	No	No	No	No	No	-4.88 cm/s
<b>1'8-cineole</b>	High	Yes	No	No	No	No	No	No	-5.30 cm/s
<b>Geraniol</b>	High	Yes	No	No	No	No	No	No	-4.11cm/s
<b><math>\gamma</math>-terpinene</b>	High	Yes	No	No	No	No	No	No	-4.70 cm/s
<b>Limonene</b>	High	Yes	No	No	No	No	No	No	-3.94 cm/s
<b>Linalool</b>	Low	Yes	No	No	No	Yes	No	No	-3.89 cm/s
<b>Nerol</b>	High	Yes	No	No	No	No	No	No	-5.13cm/s
<b>P-cymene</b>	High	Yes	No	No	No	No	No	No	-4.71cm/s
<b>Piperitone</b>	Low	Yes	No	No	No	No	Yes	No	-4.12 cm/s
<b>Sabinene</b>	High	Yes	No	No	No	No	No	No	-5.71cm/s
<b>Tagetonol</b>	Low	Yes	No	No	No	No	No	No	-4.94 cm/s
<b>Terpinen-4-ol</b>	Low	Yes	No	No	No	No	No	No	-3.94 cm/s

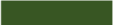



<b>(Z)-linalool oxide</b>	High	Yes	No	No	No	No	No	No	-5.61 cm/s
<b>allo-Aromadendrene</b>	Low	Yes	No	Yes	Yes	Yes	No	No	-4.20 cm/s
<b>(E)-nerolidol</b>	Low	No	No	No	Yes	Yes	No	No	-4.44 cm/s
<b><math>\alpha</math>-Amyrins</b>	High	Yes	No	Yes	No	Yes	No	No	-4.23 cm/s
<b>lupeol</b>	Low	no	no	no	no	no	no	no	-2.51 cm/s
<b>Cis-ocimene</b>	Low	No	No	No	No	No	No	No	-1.90 cm/s
<b>Cuminal</b>	High	Yes	Yes	Yes	Yes	No	No	Yes	-5.17 cm/s
<b>Cinmaldehyde</b>	High	No	No	Yes	No	Yes	Yes	Yes	-6.32 cm/s
<b>Phellanderol</b>	High	Yes	No	Yes	Yes	No	Yes	Yes	-5.81 cm/s
<b>2-tridecanone</b>	High	Yes	Yes	Yes	Yes	No	No	No	-5.17 cm/s
<b>Umbelliferone</b>	High	Yes	No	Yes	Yes	Yes	Yes	Yes	-5.87 cm/s
<b>Bargaptin</b>	High	Yes	No	Yes	No	No	No	No	-5.26 cm/s
<b>3,5-diacetylTamulin</b>	High	Yes	No	Yes	No	No	No	No	-5.52 cm/s
<b>Kaempferol</b>	High	Yes	No	Yes	No	No	No	No	-5.76 cm/s
<b>Tambulin</b>	High	Yes	No	No	No	No	No	No	-5.32 cm/s
<b>Tambuletin</b>	High	Yes	No	Yes	No	No	No	No	-3.84 cm/s
<b>Artesunate</b>	High	No	No	No	No	No	No	No	-7.31
<b>Sulfadoxine</b>	High	Yes	No	No	No	No	No	No	-5.07 cm/s



**Table 3.** LD50 values and toxicity potential of phytochemicals of *Z. armatum*.

Ligands	LD50 potential	Toxicity class	Mutagenicity	Hepatotoxicity	Immunotoxicity	Cytotoxicity	Carcinogenicity
$\alpha$ -Fenchol	1190 mg/kg	Class 4	0.97	0.69	0.96	0.93	0.62
$\alpha$ -Terpinene	1680 mg/kg	Class 4	0.85	0.78	0.95	0.85	0.75
$\alpha$ -Thujene	5000 mg/kg	Class 5	0.78	0.86	0.98	0.73	0.55
$\alpha$ -Thujone	500 mg/kg	Class 4	0.86	0.76	0.99	0.67	0.62
$\alpha$ -Pinene	3700 mg/kg	Class 5	0.93	0.86	0.99	0.75	0.60
$\alpha$ -Terpineol	1190 mg/kg	Class 4	0.97	0.69	0.96	0.93	0.62
$\beta$ -Terpineol	2000 mg/kg	Class 4	0.9	0.75	0.98	0.89	0.75
Citral	500 mg/kg	Class 4	0.98	0.69	0.99	0.82	0.88
Camphor	775 mg/kg	Class 4	0.94	0.72	0.96	0.61	0.68
Citronellal	2420 mg/kg	Class 5	0.99	0.70	0.99	0.82	0.83
Citronellol	3450 mg/kg	Class 5	0.96	0.84	0.99	0.86	0.65
1,8-cineole	2480 mg/kg	Class 5	0.96	0.86	0.99	0.75	0.68
Cis-ocimene	113 mg/kg	Class 3	0.90	0.83	0.99	0.75	0.51
Geraniol	2100 mg/kg	Class 5	0.97	0.79	0.99	0.85	0.76
$\gamma$ -terpinene	2500 mg/kg	Class 5	0.92	0.83	0.98	0.82	0.60
Limonene	4400mg/kg	Class 5	0.97	0.76	0.95	0.82	0.65
Linalool	2200mg/kg	Class 5	0.95	0.76	0.99	0.82	0.64
Nerol	2100mg/kg	Class 5	0.97	0.79	0.99	0.85	0.76
P-cymene	3 mg/kg	Class 1	0.98	0.87	0.99	0.89	0.67
Piperitone	2450 mg/kg	Class 5	0.93	0.64	0.92	0.87	0.79
Sabinene	5000 mg/kg	Class 5	0.82	0.81	0.51	0.71	0.59
Tagetonol	2500 mg/kg	Class 5	0.87	0.68	0.99	0.83	0.54
Terpinen-4-ol	1016 mg/kg	Class 4	0.83	0.80	0.99	0.88	0.72S

<b>(Z)-linalool oxide</b>	1190 mg/kg	Class 4	0.97	0.69	0.96	0.93	0.62
<b>allo-Aromadendrene</b>	1190 mg/kg	Class 4	0.97	0.69	0.96	0.93	0.62
<b><math>\beta</math>-caryophyllene</b>	1190 mg/kg	Class 4	0.97	0.69	0.96	0.93	0.62
<b>(E)-nerolidol</b>	5000 mg/kg	Class 5	0.91	0.81	0.99	0.81	0.65
<b><math>\alpha</math>-Amyrins</b>	70000 mg/kg	Class 6	0.92	0.75	0.98	0.95	0.63
<b>lupeol</b>	1190 mg/kg	Class 4	0.95	0.91	0.57	0.97	0.63
<b>Cuminal</b>	1320 mg/kg	Class 4	0.97	0.71	0.96	0.89	0.52
<b>Cinamaldehyde</b>	1850 mg/kg	Class 4	0.72	0.70	0.98	0.92	0.71
<b>Phellandral</b>	2300 mg/kg	Class 5	0.93	0.66	0.97	0.82	0.77
<b>2-Tridecanone</b>	5000 mg/kg	Class 5	0.97	0.69	0.99	0.73	0.63
<b>Umbelliferon</b>	10000 mg/kg	Class 6	0.83	0.68	0.97	0.68	0.64
<b>Bergapten</b>	8100 mg/kg	Class 6	0.75	0.79	0.83	0.85	0.84
<b>3,5-diacetylTambulin</b>	5000 mg/kg	Class 5	0.68	0.73	0.90	0.76	0.54
<b>Kaempferol</b>	3919 mg/kg	Class 5	0.52	0.68	0.96	0.98	0.72
<b>Tambuletin</b>	5000 mg/kg	Class 5	0.77	0.83	0.98	0.50	0.93
<b>Tambulin</b>	3919 mg/kg	Class 5	0.77	0.70	0.87	0.66	0.63
<b>Artesunate</b>	1000 mg/kg	Class 4	0.63	0.76	0.87	0.87	0.65
<b>Sulfadoxine</b>	5200 mg/kg	Class 6	0.72	0.50	0.99	0.93	0.52

	Strongly non-toxic
	Less non-toxic
	Less toxic
	Strongly toxic

Analysis of LD50 values revealed that  $\alpha$ -Amyrins shows 70000mg/kg and class VI, Bergapten and Umbelliferon have high LD50 values (8100 and 10000 mg/kg) therefore, belong to class 6 that is nontoxic, Sabinene have 5000mg/kg and Phellandral have 2300mg/kg are categorized in class 5. Cuminal is placed in class 4 that could be harmful if swallowed have value of 1850mg/kg and P-Cymene belongs to class 1 have value 3mg/kg that is highly toxic. The details of all the compounds are presented in Table 3.

Based on pharmacokinetics analysis, various compounds that showed more than one Lipinski's violations, less bioactivity score and toxic potential were filtered out and the remaining compounds were selected for the molecular docking studies. The schematic representation of the study is shown in graphical abstract.

### Molecular Docking

After the initial analysis, 21 phytochemicals were selected for further analysis and docked with 3 target proteins involved in the pathogenesis of malaria with the help of AutoDock vina v1.5.6. PfAMA-1 (1Z40) showed the highest binding affinities with Cuminal (-5.9Kcal/mol), Pf GST (1OKT) exhibited the highest binding interaction with Sabinene (-7.1 Kcal/mol), while PfDHFR (7F3Y) showed the highest binding affinities with Phellandral (-5.5 Kcal/mol) (Tables 4, 5 and 6; Figures 2 and 3).

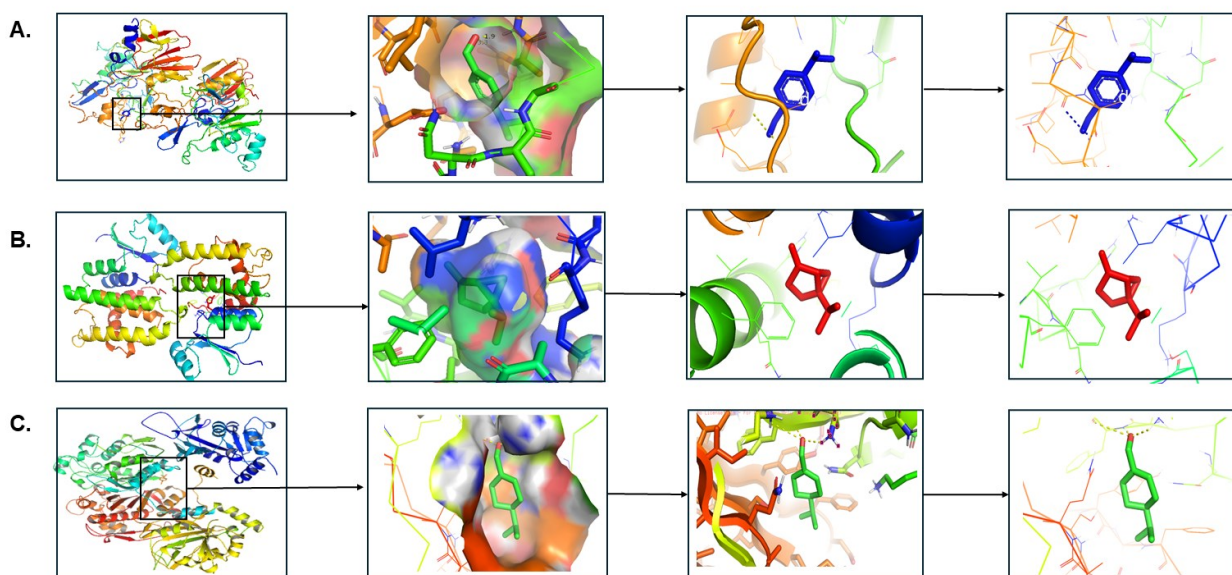


**Figure 2.** Different interactive docked poses of the selected phytochemical from *Z. armatum*. **A.** Pf Anti-Malarial Antigen1(Pf AMA1) with Cuminal, **B.** Pf Glutathione S-Transferase (Pf GST) with Sabinene **C.** Pf dihydrofolate reductase-thymidylate synthase (Pf DHFR-TS) with Phellandral.

Cuminal shows 3 amino acid interaction GLU350 (Conventional hydrogen bonding), PRO350 (Pi-Alkyl) And GLU365 (Pi-Anion). Sabinene shows an interaction with ALA164, LEU18, VAL103, HIS107, PHE100, LYS15 (Conventional

hydrogen bonding). Phellandral shows interactions with PHE499, TYR497(both with Pi-Alkyl) and PHE354 (Conventional hydrogen bonding). Sulfadoxine and Artesunate was used as standard drugs, sulfadoxine show no interaction with PfAMA-1 (1Z40) and PfGST (1OKT) but with Pf-Dihydrofolate reductase (7F3Y) as LYS353, GLN542 (both are conventional hydrogen bonding), LYS502, TYR497, SER504, ASN340, LYS359 (Pi-Anion). Artesunate show binding affinity with PfAMA-1 (1Z40) is -9.0 kcal/mol as PRO330, ARG128, SER392, LYS351, SER347, LYS395, TYR397, with Pf GST (1OKT) is -7.8 kcal/mol and interactions are ALA12, TYR211, VAL210, PHE10, LEU10, ALA41, PHE42, *ASP11* and with Pf-Dihydrofolate reductase (7F3Y) is -7.0 kcal/mol with interactions are PHE354, PHE499, LYS502, SER504, LYS302. It shows conventional hydrogen bonding, Pi-Anion and Pi-Alkyl, carbon hydrogen bonding and alkyl bonding. It only shows only unfavorable donor donor interaction with PfAMA-1 (1Z40). The docking poses of all the other phytochemicals are shown in tables 4, 5 and 6.

**Table 4.** Binding affinities of PfAMA-1 (1Z40) with selected phytochemicals from *Z. armatum*

Ligands	Binding Affinities Kcal/mol	Receptor protein	Interacting Amino acids residues
$\alpha$ -Terpinene	-5.4	PfAMA-1	PRO350, GLU365
$\alpha$ -pinene	-5.5	PfAMA-1	LYS364, LYS391, ARG389, ARG143, TYR390, LEU380
$\beta$ -Terpineol	-5.6	PfAMA-1	PRO381, LEU380, ASP134, LYS391, ARG143, TYR390
Citral	-5.0	PfAMA-1	ILE332, TYR397, LYS351, LEU340, PHE329, PRO330
Citronellol	-4.6	PfAMA-1	SER345, LYS351, LEU340, PHE329, PRO330
Citronellal	-4.6	PfAMA-1	LYS364, ARG143, LEU380, ILE363, TYR360, ARG389, TYR390, LYS391
1'8-cineole	-5.6	PfAMA-1	ARG143, LYS364, LEU380, ARG389, TYR390
Cis-ocimene	-4.8	PfAMA-1	LEU380, ARG143, LYS364, ARG389, TYR390, LYS391
Geraniol	-4.8	PfAMA-1	LEU380, ARG143, LYS364, LYS391, TYR390
$\gamma$ - terpinene	-5.6	PfAMA-1	GLU365, LEU357
Limonene	-5.1	PfAMA-1	LEU380, ARG143, LYS391, TYR390, ARG389
Linalool	-4.8	PfAMA-1	PRO330, LYS351, PHE329, LEU340, TYR397, LEU344
Nerol	-4.7	PfAMA-1	PHE329, PRO330, LYS351, LEU340, SER347
Piperitone	-5.4	PfAMA-1	ARG143, LYS391, LYS364, TYR390, LEU380
Sabinene	-5.6	PfAMA-1	LYS364, ARG143, LYS391, TYR390, ARG389
Tagetonol	-4.8	PfAMA-1	PRO330, LEU340, LEU344, TYR397, GLU336, ILE332
(E)-nerolidol	-5.7	PfAMA-1	LEU340, PHE329, PRO330, PRO350, LYS391
Cuminal	-5.9	PfAMA-1	PRO350, GLU354, GLU365
Phellandral	-5.5	PfAMA-1	LUE357, PRO330
2-tridecanone	-4.5	PfAMA-1	PRO330, TYR397, LEU340, LYS351
Sulfadoxine	-3.8	PfAMA-1	No interaction
Artesunate	-9.0	PfAMA-1	PHE354, PHE499, LYS502, SER504, LYS302

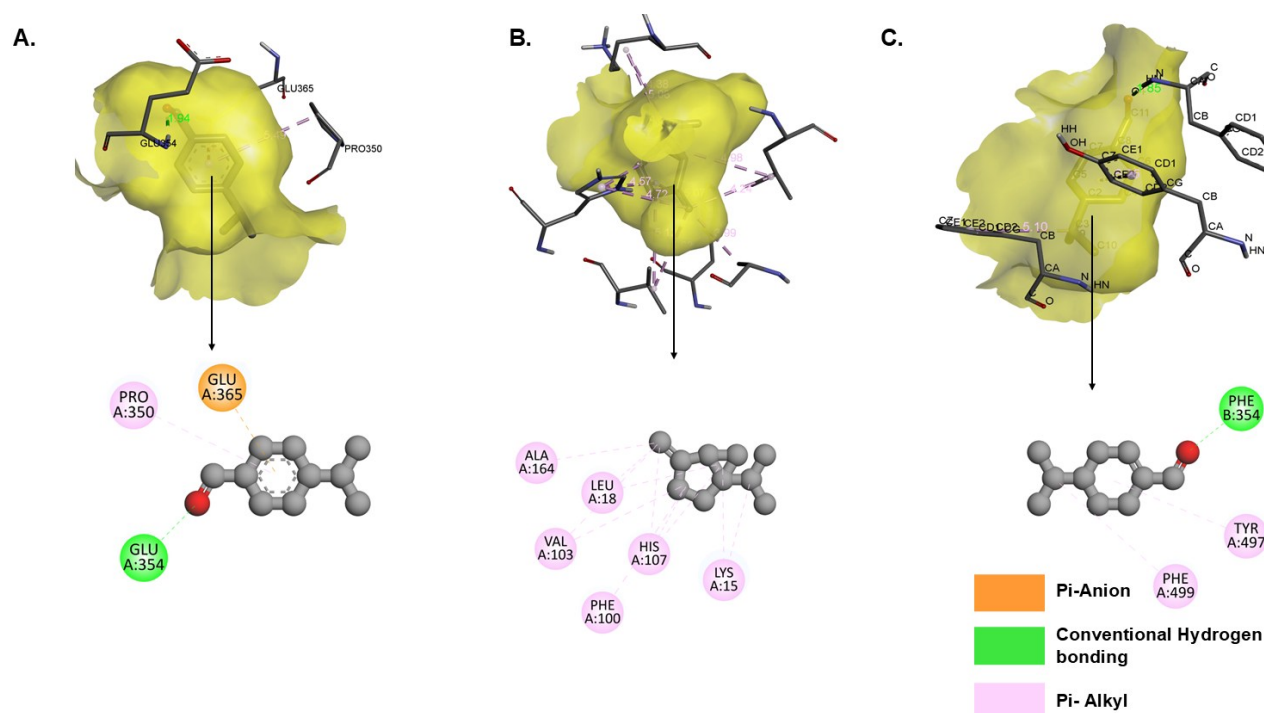


**Figure 3.** Molecular docking representations showing the interaction of selected phytochemicals from *Z. armatum* with key *Plasmodium falciparum* receptor proteins involved in malaria pathogenesis. **A.** Pf Anti-Malarial Antigen1 (Pf AMA-1) with Cuminal, **B.** Pf Glutathione S-Transferase (Pf GST) with Sabinene **C.** Pf dihydrofolate reductase-thymidylate synthase (Pf DHFR-TS) with Phellandral. These docked complexes highlight the potential of *Z. armatum* phytoconstituents as anti-malarial agents through multi-target inhibition.

**Table 5.** Docking analysis of Pf GST with selected phytochemicals of *Z. armatum*.

Ligand	Protein (10KT)	Binding affinity Kcal/mol	Amino acids residues interaction
1,8-cineole	Pf GST	-6.3	TYR211, ALA12, ALA41, PHE42, PHE10, LEU115
2-tridecanone	Pf GST	-4.8	PHE10, TYR211, LEU215, ALA12, PHE42, ALA41
$\alpha$ -Terpinene	Pf GST	-6.3	HIS107, PHE116, LYS15, GLN104, LEU118
$\alpha$ -Pinene	Pf GST	-6.8	VAL76, VAL103, LEU18, PHE100, HIS107
$\beta$ -Terpineol	Pf GST	-6.0	HIS107, LYS15, PHE116, PHE100, LEU18
Cis-ocimene	Pf GST	-6.1	VAL103, VAL76, HIS107, TYR108, PHE116, PHE100, LEU18, LYS15
Citral	Pf GST	-5.3	PHE10, PHE42, LEU115, LYS175, TYR211, ALA12, TYR176
Citronellal	Pf GST	-5.6	LYS15, PHE176, HIS107
Citronellol	Pf GST	-5.0	PH10, PHE42, ALA12, ALA41, TYR176, TYR211, LEU115
Cuminal	Pf GST	-6.3	PHE45, GLN18
(E)-nerolidol	Pf GST	-6.9	TYE108, LYS15, PHE116, PHE100, HIS160, ALA164, LEU18, VAL103, HIS107
$\gamma$ -terpinene	Pf GST	-6.4	PHE116, PHE100, GLN104, LEU18, LYS15
Geraniol	Pf GST	-5.8	TYR108, PHE116, HIS 107, LYS15, PHE 100
Limonene	Pf GST	-6.3	HIS107, LEU18, PHE116, PHE100, VAL76, LYS 15



<b>Linalool</b>	<i>Pf</i> GST	-5.4	TYR211, LEU215, TYR211, ASN 111, LYS175, PHE110
<b>Nerol</b>	<i>Pf</i> GST	-6.1	PHE100, PHE116, TYR108, HIS107, LYS15, GLY14(UNFAVORABLE ACCEPTOR-ACCEPTOR)
<b>Phellandral</b>	<i>Pf</i> GST	-6.3	PHE100, LYS15, LEU18, GLN104
<b>Piperitone</b>	<i>Pf</i> GST	-6.5	LYS15, LUE18, PHE116
<b>Sabinene</b>	<i>Pf</i> GST	-7.1	ASN 111, PHE110, LYS175
<b>Tagetonol</b>	<i>Pf</i> GST	-5.1	ASN111, TYR21, PHE110
<b>Artesunate</b>	<i>Pf</i> GST	-7.8	ALA12, TYR211, VAL210, PHE10, LEU10, ALA41, PHE42, ASP11(UNFAVORABLE ACCEPTOR-ACCEPTOR)
<b>Sulfadoxine</b>	<i>Pf</i> GST	-4.7	No interaction

**Table 6.** Docking analysis of *Pf*-DHFR with selected phytochemicals of *Z. armatum*.

<b>Ligand</b>	<b>Binding affinities kcal/mol</b>	<b>Receptor (7F3Y)</b>	<b>Interactions</b>
<b>1,8-cineole</b>	-5.3	<i>Pf</i> -DHFR	ALA541, LYS353, ASN340, TYR497, PHE499
<b>2-Tridecanone</b>	-3.6	<i>Pf</i> -DHFR	ALA541, LYS502, SER504
<b><math>\alpha</math>-Terpinene</b>	-5.2	<i>Pf</i> -DHFR	LYS353, TYR497, LYS502, ALA541
<b><math>\alpha</math>-Pinene</b>	-5.2	<i>Pf</i> -DHFR	LYS353, TYR497, LYS502, ALA541
<b><math>\beta</math>-Terpineol</b>	-4.5	<i>Pf</i> -DHFR	PHE499, PHE353, LYS 353, TYR497, LYS502, ALA541
<b>Cis-ocimene</b>	-5.4	<i>Pf</i> -DHFR	ALA541, LYS502, TYR497
<b>Citral</b>	-4.5	<i>Pf</i> -DHFR	ALA541, LYS502
<b>Citronellal</b>	-4.4	<i>Pf</i> -DHFR	ALA541, LYS502, PHE354, LYS353, GLN542, TYR497, PHE499
<b>Citronellol</b>	-4.2	<i>Pf</i> -DHFR	LYS353, TYR497, ALA541, LYS502
<b>Cuminal</b>	-5.3	<i>Pf</i> -DHFR	ASN340, PHE499, GLN542, LYS353, PHE354
<b>(E)-nerolidol</b>	-5.0	<i>Pf</i> -DHFR	PHE499, LYS502, LYS353, GLN542, SER504, TYR497, ALA541
<b><math>\gamma</math>-terpinene</b>	-5.2	<i>Pf</i> -DHFR	LYS353, PHE499, ASN340
<b>Geraniol</b>	-4.5	<i>Pf</i> -DHFR	LYS353, TYR497, PHE499, LYS502
<b>Limonene</b>	-5.2	<i>Pf</i> -DHFR	ALA541, TYR497, LYS502, PHE499, LYS353
<b>Linalool</b>	-4.3	<i>Pf</i> -DHFR	ALA541, TYR497, LYS502, PHE499, LYS353, PHE354
<b>Nerol</b>	-4.4	<i>Pf</i> -DHFR	TYR497, PHE499, LYS502
<b>Phellandral</b>	-5.5	<i>Pf</i> -DHFR	PHE354, PHE499, TYR457
<b>Piperitone</b>	-5.4	<i>Pf</i> -DHFR	LYS502, ALA541, TYR497, SER504, LYS353
<b>Sabinene</b>	-5.0	<i>Pf</i> -DHFR	LYS353, TYR497, PHE499
<b>Tagetonol</b>	-5.0	<i>Pf</i> -DHFR	TYR497, LYS353, ALA514
<b>Sulfadoxine</b>	-6.4	<i>Pf</i> -DHFR	LYS353, GLN542, LYS502, TYR497, SER504, ASN340, LYS359, LYS353
<b>Artesunate</b>	-7.0	<i>Pf</i> -DHFR	PHE354, SER504, LYS302, LYS 502, PHE499

## Molecular Dynamic Simulations

The structural flexibility of the best docked complexes (highest binding affinities) was evaluated by GROMACS. On the basis of the results, the variation of Rg is caused by protein-ligand interactions of their binding sites. Rg is Radius of Gyration that describes protein compactness and stability in MD simulation. The Rg plots evaluate the protein structure's compactness over time. In the Sabinene–PfGST complex, the Rg remains consistently between approximately 2.555 and 2.565 nm, indicating that the protein maintains its structural integrity and stable tertiary conformation (Figure 5B). Likewise, the Cuminal complex exhibits minor variations, showing no significant signs of unfolding or collapse in the protein (Figure 4B). On the other hand, the Phellandral complex shows a gradual decline in Rg values from initial measurements to a stable range of 3.28–3.32 nm, suggesting that the protein becomes more compact following ligand binding (Figure 6B). This compaction signifies improved stability upon the formation of the complex.

The RMSD graphs for the three ligands Cuminal, Sabinene, and Phellandral demonstrate overall structural stability throughout the 50 ns MD simulation. The Sabinene–Pf GST complex displays the most stable pattern, with RMSD values slightly varying between 0.25 and 0.35 nm, indicating consistent ligand binding without significant conformational alterations (Figure 5A). Pf AMA-1 Cuminal's RMSD shows a comparable trend, achieving stability around 0.3–0.5 nm after some initial minor fluctuations (Figure 4A). The Phellandral–Pf DHFR complex experiences an initial increase in RMSD during the first 5 ns but subsequently stabilizes between 0.6 and 0.7 nm (Figure 6A), suggesting the system has reached equilibrium and that binding is thermodynamically favorable across all complexes.

SASA measurements offer insight into how much protein surface is accessible to the solvent. In the Sabinene complex, the SASA values hover around 230–235 nm<sup>2</sup>, indicating that there has been no notable unfolding or exposure of hydrophobic areas (Figure 5C). A similar pattern is seen in the Cuminal–Pf AMA-1 complex, where stable SASA values demonstrate structural integrity and minimal changes in conformation (Figure 4C). Conversely, the Phellandral–Pf DHFR complex exhibits a downward trend in SASA over time, suggesting a decrease in solvent-accessible surface area due to enhanced compactness and stabilization of the protein structure (Figure 6C).

The RMSF analysis assesses the variability of individual amino acid residues. For all three complexes, minimal fluctuations are noted across most residues (<0.3 nm), especially in the regions of the active site, suggesting robust stabilization induced by the ligands. Somewhat increased fluctuations are confined to the terminal and loop regions, which is commonly observed in such simulations. The stability observed in the core and binding-site residues of the Cuminal, Sabinene, and Phellandral complexes supports their effective interaction and potential as promising bioactive antimalarial agents targeting Pf GST. The highest peak was observed for Cuminal at 350–400 residue index at 0.34 nm (Figure 4D). For sabinene it was from

0 -50 at 37nm (Figure 5D). For Phellandral it was observed at 600 residue index at 0.75nm (Figure 6D).

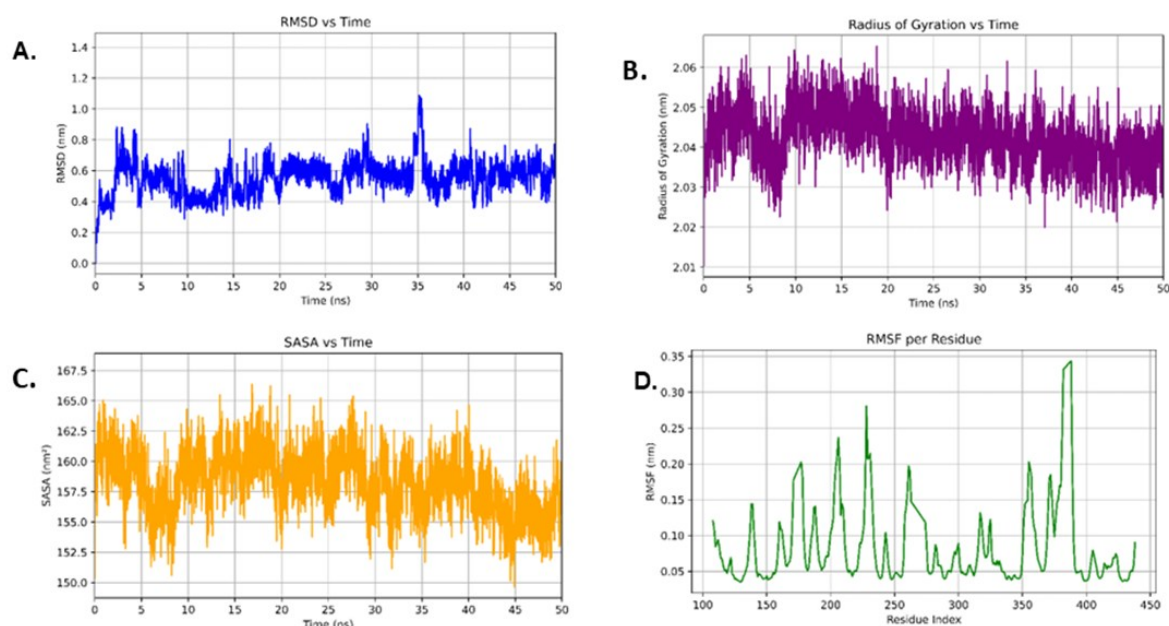


**Figure 4.** Molecular dynamics simulation analysis of the Cuminal-PfAMA1 complex. **A.** RMSD (Root Mean Square Deviation) vs Time plot indicates the overall stability of the protein-ligand complex across the 50 ns simulation, showing relatively stable fluctuations within an acceptable range. **B.** Radius of Gyration vs Time assesses the compactness of the protein structure, demonstrating minor variations and maintaining structural integrity. **C.** SASA (Solvent Accessible Surface Area) vs Time reveals slight fluctuations in the protein's surface exposure to solvent, suggesting consistent folding behaviour. **D.** RMSF (Root Mean Square Fluctuation) per Residue identifies flexible regions in the PfAMA-1 protein, with higher peaks corresponding to terminal or loop regions). Together, these results confirm the dynamic stability and structural compatibility of Cuminal with PfAMA-1

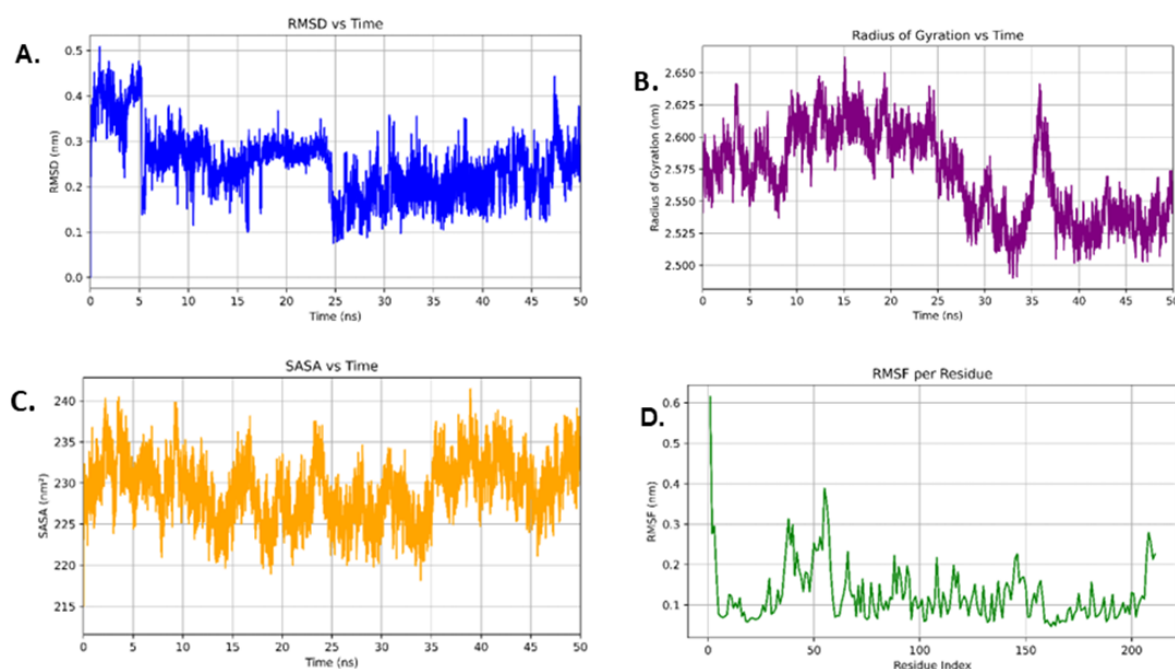


**Figure 5.** Molecular dynamics simulation analysis of the Sabinene-PfGST complex. **A.** RMSD vs Time plot demonstrates the structural stability of the protein-ligand complex, with consistent fluctuations indicating a relatively stable interaction over the 50 ns simulation. **B.** Radius of Gyration vs Time reflects the compactness of the protein, indicating moderate conformational changes but overall maintenance of structural integrity. **C.** SASA vs Time reveals fluctuations in solvent-accessible surface area, signifying stable surface exposure over time. **D.** RMSF per Residue highlights residue-level flexibility, with higher peaks suggesting more dynamic regions, possibly at terminal loops or active sites. These results collectively suggest a stable binding of Sabinene to PfGST, with acceptable dynamic behavior throughout the simulation.

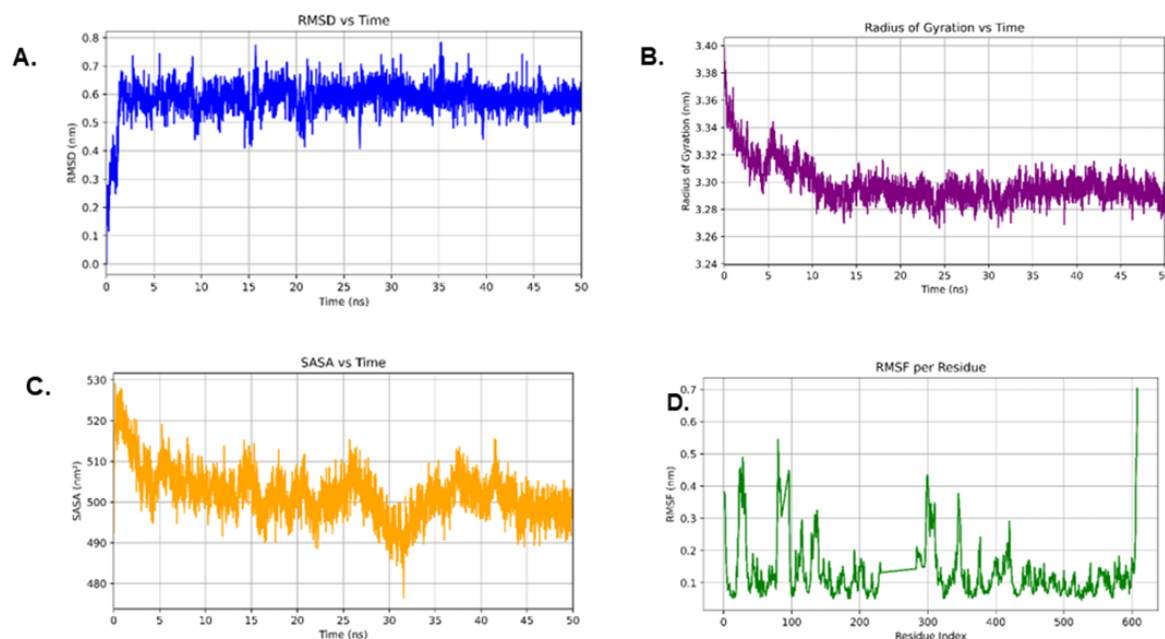


**Figure 6.** Molecular dynamics simulation analysis of the Phellandral-PfDHFR-TS complex. **A.** RMSD vs Time plot shows the backbone stability of the protein-ligand complex, with the RMSD stabilizing around 0.4–0.6 nm after initial fluctuations, indicating conformational stability. **B.** Radius of Gyration vs Time indicates compactness of the protein structure, showing a steady decline and plateau, reflecting structural tightening upon ligand binding. **C.** SASA vs Time represents the solvent-accessible surface area, which remains consistent with moderate fluctuations, implying stable solvent exposure. **D.** RMSF per Residue depicts the flexibility of individual residues, with minor peaks indicating local flexibility in

terminal or loop regions. These parameters collectively suggest that Phellandral maintains a stable interaction with PfDHFR-TS throughout the simulation.

## Network Pharmacology

### *Identification of Potential Targets Through Network Pharmacology Analysis*

Network pharmacology is a multidisciplinary approach that explores the interactions of biological systems, drugs and diseases to provide a holistic view of drug action and identify potential therapeutic effects (Hopkins, 2007). We have found 5383 potential malaria targets from Gene card and DesGenet and, after elimination and integration, 240 were selected. Swiss target database revealed 99 malarial targets of the 3 selected phytochemicals (Cuminal, Sabinene, and Phellandral). On removal of duplicates and the addition of malarial-associated targets 23 common targets were found, that represent probable overlap between compounds and the disease targets (Supplementary table 7). These shared proteins were considered as potential targets of the chosen plant-based molecules against malaria (Figure 7A). A protein-protein interaction network identified the connections between various proteins within a cell that are crucial for insight into cellular functions and disease mechanisms (Wang et al., 2022; 2023).

### *Compound Target Network Interactions*

The compound-target network was constructed using Cytoscape to analyze the interaction between the 3 active compounds and their potential targets (Figure B7). The interaction analysis showed that one active ingredient can affect multiple targets, while the same target may interact with more than one active compound. This reflects the multi-target and multi-components effects of the phytochemicals for the treatment of malaria.

### *Construction of Protein–Protein Interaction (PPI) Network and Hub Genes*

The Protein–protein-Interaction network of 23 common target genes was constructed using STRING database (Figure 7C). After visualizing the PPI network in Cytoscape, 185 nodes with 300 edges were found (Figure 7D). The CytoHubba plugin was employed to identify hub genes and among the 12 available methods the degree method was chosen to identify the top ranked hub genes. The following genes, MPO, TNF, IL6, ALB, HMOX1, GSR, NOS2, IDO1, CXCL8, and PTPRC have emerged as the top-ranked genes due to their significantly high values. After the identification of the first stage node genes, Cuminal was found effective against ALB, MPO, PTPRC, CXCL8, NOS2, HMOX1 and GSR.



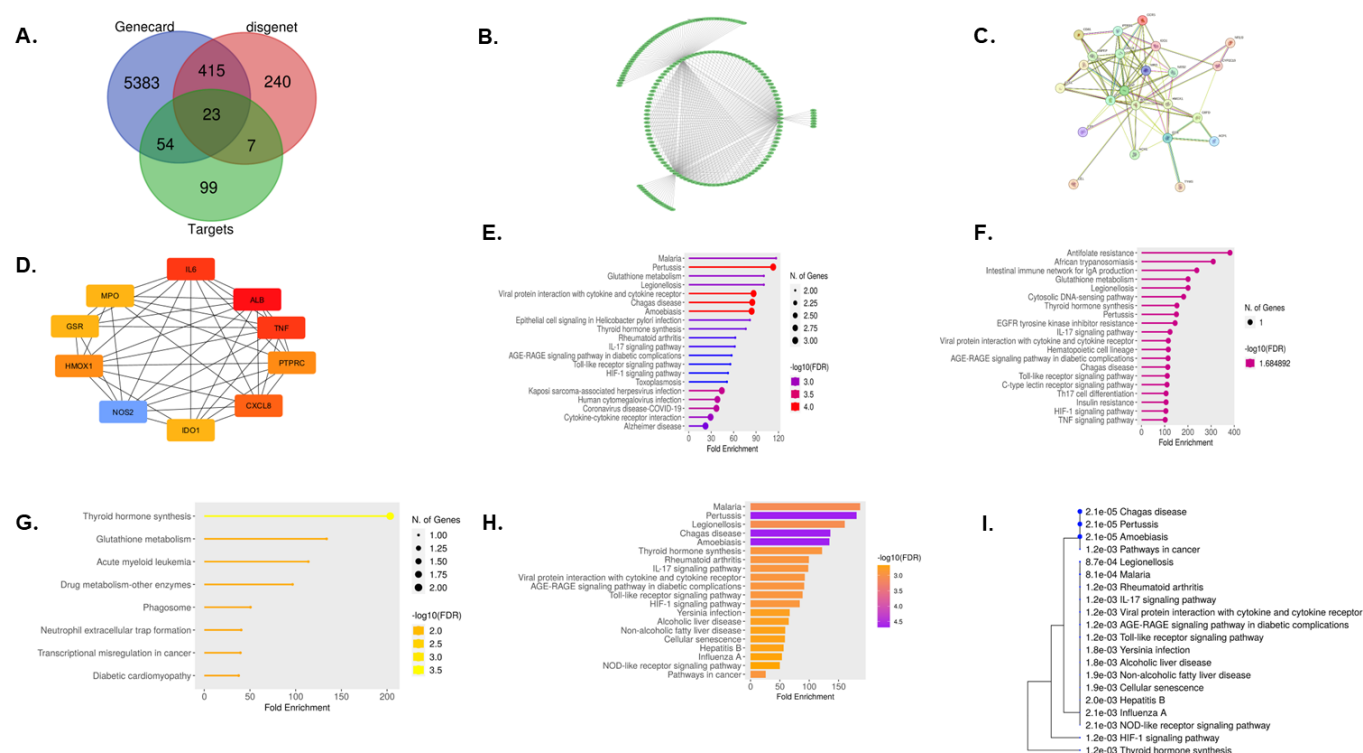


**Figure 7.** **A.** The diagrammatic representation of Venn diagram of target genes and 3 Drug targets from Genecards, DisGenet and Swisstar prediction data. **B.** The Cytoscape analysis representing compound target pathway network of related targets and genes. **C.** String Database representing protein-protein interactions of compound target. **D.** The top 10 hub genes from CytoHubba plugin of Cytoscape analysis. **E.** David Database represents Gene ontology plots of biological process of top 10 hub genes from Cytoscape analysis. **F.** David Database represents Gene ontology plots of Cellular Components of top 10 hub genes from Cytoscape analysis. **G.** David Database represents Gene ontology plots Molecular function of top 10 hub genes from Cytoscape analysis. **H.** Enrichment analyses of targeted genes including KEGG pathways. **I.** Enrichment analysis of targeted genes clustering between pathways.

### Gene Ontology and Pathway Enrichment Analysis

Gene Ontology is a structured and standardized system used to categorize and describe the functions of genes and their products (Zhou et al., 2017) to identify the molecular mechanisms of active compounds, GO annotations and analysis of the KEGG pathway were carried out on a set of 99 targets associated with malaria. The GO analysis recognized various biological processes (BP) (Figure 7E), which include the regulation of malaria disease, the transport system, the positive regulation of cell communication, the positive regulation of signaling pathways, the regulation of programmed cell death and blood circulation; two cellular components (CC) (Figure 7F), including extracellular exosomes, membrane raft and one molecular function (MF) (Figure 7G) such as cytokine activity. The cutoff value of  $P < 0.05$  was applied to select top 20 GO annotations (BP, CC, MF) and lollipop plots were drawn.

KEGG analysis predicted eight pathways associated with significant fold enrichment values and false discovery rate, such as malaria, pertussis and Chagas disease, indicating a strong involvement of these pathways in infectious diseases; other pathways include thyroid hormone synthesis, IL-17, and the AGE-RAGE signaling pathway involved in diabetic complications, metabolic regulations, and immune response (Figure 7H). A hierarchical clustering tree was constructed to

**A.**

Yersinia infection  
with cytokine and chemokine receptor disease  
Alcoholic liver disease  
Pathways in cancer  
Hepatitis B  
Legionnaires disease  
HIF-1 signaling pathway  
Pertussis  
Influenza A  
IL-17 signaling pathway  
NOD-like receptor signaling pathway  
Toll-like receptor signaling pathway  
Cellular senescence  
Amoebiasis  
Malaria  
Rheumatoid arthritis  
AGE-RAGE signaling pathway in diabetic complications  
Viral protein interaction with cytokine and chemokine receptor disease

**B.**

IL-17 signaling pathway  
IL-17 receptor  
IL-17A  
IL-17F  
IL-17RA  
IL-17RB  
IL-17RC  
IL-17RD  
IL-17RE  
IL-17RF  
IL-17RG  
IL-17RH  
IL-17RI  
IL-17RII  
IL-17RIII  
IL-17RIV  
IL-17RV  
IL-17RW  
IL-17RX  
IL-17RY  
IL-17RZ  
IL-17RA1  
IL-17RA2  
IL-17RA3  
IL-17RA4  
IL-17RA5  
IL-17RA6  
IL-17RA7  
IL-17RA8  
IL-17RA9  
IL-17RA10  
IL-17RA11  
IL-17RA12  
IL-17RA13  
IL-17RA14  
IL-17RA15  
IL-17RA16  
IL-17RA17  
IL-17RA18  
IL-17RA19  
IL-17RA20  
IL-17RA21  
IL-17RA22  
IL-17RA23  
IL-17RA24  
IL-17RA25  
IL-17RA26  
IL-17RA27  
IL-17RA28  
IL-17RA29  
IL-17RA30  
IL-17RA31  
IL-17RA32  
IL-17RA33  
IL-17RA34  
IL-17RA35  
IL-17RA36  
IL-17RA37  
IL-17RA38  
IL-17RA39  
IL-17RA40  
IL-17RA41  
IL-17RA42  
IL-17RA43  
IL-17RA44  
IL-17RA45  
IL-17RA46  
IL-17RA47  
IL-17RA48  
IL-17RA49  
IL-17RA50  
IL-17RA51  
IL-17RA52  
IL-17RA53  
IL-17RA54  
IL-17RA55  
IL-17RA56  
IL-17RA57  
IL-17RA58  
IL-17RA59  
IL-17RA60  
IL-17RA61  
IL-17RA62  
IL-17RA63  
IL-17RA64  
IL-17RA65  
IL-17RA66  
IL-17RA67  
IL-17RA68  
IL-17RA69  
IL-17RA70  
IL-17RA71  
IL-17RA72  
IL-17RA73  
IL-17RA74  
IL-17RA75  
IL-17RA76  
IL-17RA77  
IL-17RA78  
IL-17RA79  
IL-17RA80  
IL-17RA81  
IL-17RA82  
IL-17RA83  
IL-17RA84  
IL-17RA85  
IL-17RA86  
IL-17RA87  
IL-17RA88  
IL-17RA89  
IL-17RA90  
IL-17RA91  
IL-17RA92  
IL-17RA93  
IL-17RA94  
IL-17RA95  
IL-17RA96  
IL-17RA97  
IL-17RA98  
IL-17RA99  
IL-17RA100  
IL-17RA101  
IL-17RA102  
IL-17RA103  
IL-17RA104  
IL-17RA105  
IL-17RA106  
IL-17RA107  
IL-17RA108  
IL-17RA109  
IL-17RA110  
IL-17RA111  
IL-17RA112  
IL-17RA113  
IL-17RA114  
IL-17RA115  
IL-17RA116  
IL-17RA117  
IL-17RA118  
IL-17RA119  
IL-17RA120  
IL-17RA121  
IL-17RA122  
IL-17RA123  
IL-17RA124  
IL-17RA125  
IL-17RA126  
IL-17RA127  
IL-17RA128  
IL-17RA129  
IL-17RA130  
IL-17RA131  
IL-17RA132  
IL-17RA133  
IL-17RA134  
IL-17RA135  
IL-17RA136  
IL-17RA137  
IL-17RA138  
IL-17RA139  
IL-17RA140  
IL-17RA141  
IL-17RA142  
IL-17RA143  
IL-17RA144  
IL-17RA145  
IL-17RA146  
IL-17RA147  
IL-17RA148  
IL-17RA149  
IL-17RA150  
IL-17RA151  
IL-17RA152  
IL-17RA153  
IL-17RA154  
IL-17RA155  
IL-17RA156  
IL-17RA157  
IL-17RA158  
IL-17RA159  
IL-17RA160  
IL-17RA161  
IL-17RA162  
IL-17RA163  
IL-17RA164  
IL-17RA165  
IL-17RA166  
IL-17RA167  
IL-17RA168  
IL-17RA169  
IL-17RA170  
IL-17RA171  
IL-17RA172  
IL-17RA173  
IL-17RA174  
IL-17RA175  
IL-17RA176  
IL-17RA177  
IL-17RA178  
IL-17RA179  
IL-17RA180  
IL-17RA181  
IL-17RA182  
IL-17RA183  
IL-17RA184  
IL-17RA185  
IL-17RA186  
IL-17RA187  
IL-17RA188  
IL-17RA189  
IL-17RA190  
IL-17RA191  
IL-17RA192  
IL-17RA193  
IL-17RA194  
IL-17RA195  
IL-17RA196  
IL-17RA197  
IL-17RA198  
IL-17RA199  
IL-17RA200  
IL-17RA201  
IL-17RA202  
IL-17RA203  
IL-17RA204  
IL-17RA205  
IL-17RA206  
IL-17RA207  
IL-17RA208  
IL-17RA209  
IL-17RA210  
IL-17RA211  
IL-17RA212  
IL-17RA213  
IL-17RA214  
IL-17RA215  
IL-17RA216  
IL-17RA217  
IL-17RA218  
IL-17RA219  
IL-17RA220  
IL-17RA221  
IL-17RA222  
IL-17RA223  
IL-17RA224  
IL-17RA225  
IL-17RA226  
IL-17RA227  
IL-17RA228  
IL-17RA229  
IL-17RA230  
IL-17RA231  
IL-17RA232  
IL-17RA233  
IL-17RA234  
IL-17RA235  
IL-17RA236  
IL-17RA237  
IL-17RA238  
IL-17RA239  
IL-17RA240  
IL-17RA241  
IL-17RA242  
IL-17RA243  
IL-17RA244  
IL-17RA245  
IL-17RA246  
IL-17RA247  
IL-17RA248  
IL-17RA249  
IL-17RA250  
IL-17RA251  
IL-17RA252  
IL-17RA253  
IL-17RA254  
IL-17RA255  
IL-17RA256  
IL-17RA257  
IL-17RA258  
IL-17RA259  
IL-17RA260  
IL-17RA261  
IL-17RA262  
IL-17RA263  
IL-17RA264  
IL-17RA265  
IL-17RA266  
IL-17RA267  
IL-17RA268  
IL-17RA269  
IL-17RA270  
IL-17RA271  
IL-17RA272  
IL-17RA273  
IL-17RA274  
IL-17RA275  
IL-17RA276  
IL-17RA277  
IL-17RA278  
IL-17RA279  
IL-17RA280  
IL-17RA281  
IL-17RA282  
IL-17RA283  
IL-17RA284  
IL-17RA285  
IL-17RA286  
IL-17RA287  
IL-17RA288  
IL-17RA289  
IL-17RA290  
IL-17RA291  
IL-17RA292  
IL-17RA293  
IL-17RA294  
IL-17RA295  
IL-17RA296  
IL-17RA297  
IL-17RA298  
IL-17RA299  
IL-17RA300  
IL-17RA301  
IL-17RA302  
IL-17RA303  
IL-17RA304  
IL-17RA305  
IL-17RA306  
IL-17RA307  
IL-17RA308  
IL-17RA309  
IL-17RA310  
IL-17RA311  
IL-17RA312  
IL-17RA313  
IL-17RA314  
IL-17RA315  
IL-17RA316  
IL-17RA317  
IL-17RA318  
IL-17RA319  
IL-17RA320  
IL-17RA321  
IL-17RA322  
IL-17RA323  
IL-17RA324  
IL-17RA325  
IL-17RA326  
IL-17RA327  
IL-17RA328  
IL-17RA329  
IL-17RA330  
IL-17RA331  
IL-17RA332  
IL-17RA333  
IL-17RA334  
IL-17RA335  
IL-17RA336  
IL-17RA337  
IL-17RA338  
IL-17RA339  
IL-17RA340  
IL-17RA341  
IL-17RA342  
IL-17RA343  
IL-17RA344  
IL-17RA345  
IL-17RA346  
IL-17RA347  
IL-17RA348  
IL-17RA349  
IL-17RA350  
IL-17RA351  
IL-17RA352  
IL-17RA353  
IL-17RA354  
IL-17RA355  
IL-17RA356  
IL-17RA357  
IL-17RA358  
IL-17RA359  
IL-17RA360  
IL-17RA361  
IL-17RA362  
IL-17RA363  
IL-17RA364  
IL-17RA365  
IL-17RA366  
IL-17RA367  
IL-17RA368  
IL-17RA369  
IL-17RA370  
IL-17RA371  
IL-17RA372  
IL-17RA373  
IL-17RA374  
IL-17RA375  
IL-17RA376  
IL-17RA377  
IL-17RA378  
IL-17RA379  
IL-17RA380  
IL-17RA381  
IL-17RA382  
IL-17RA

**Figure 8.** Enrichment analyses of targeted genes including **A.** signaling pathways and **B.** pathways interaction network

Malaria continues to be a significant global health concern, with *P. falciparum* responsible for 90% of infections and showing resistance to numerous existing medications (Muregi et al., 2011) (Kamaraj et al., 2023). Artemisinin-based combination therapies (ACTs) serve as the main treatment, merging rapidly acting ART derivatives with longer-acting partner medications. Investigating traditional medicinal plants presents a hopeful option to address the increasing issue of drug resistance (Eastman and Fidock, 2009). The combination of indigenous knowledge with rigorous scientific inquiry can pave the way for the development of novel and effective anti-malarial interventions. *Z. armatum* DC possesses a range of biological activities, including antibacterial, antifungal, antiviral, anthelmintic, cytotoxic, anti-inflammatory, mosquito larvicidal, hepatoprotective, antinociceptive, immunomodulatory, antioxidant, and cardiovascular effects (Mukhtar and Kalsi, 2018). Therefore, the present study explored the protective effects of 40 phytochemicals from *Z. armatum* against malaria via molecular docking, molecular dynamic simulations and network pharmacology analysis. We have identified three important compounds (Cuminal, Sabinene and Phellandral) in *Z. armatum* with strong anti-malarial potential by inhibiting the activity of essential proteins involved in the pathogenesis of malaria. The 40 bioactive compounds were initially

screened using Lipinski's rule of five and only one compound (Tambuletin) showed three Lipinski violations while all the other compounds adhered to the rule. According to Lipinski's rule of five, Cuminal exhibited highest binding free energy that is an indicative of its excellent bioavailability and better function when taken orally as it will be able to cross the cell membrane (Singh and Verma, 2013).

Cuminal had the most favorable binding energy among the phytochemicals that were evaluated, suggesting a robust and long-lasting interaction with the target malarial proteins. This implies that Cuminal might have strong inhibitory effects, which would make it a viable medication option. In addition to having a higher binding affinity than other substances, Cuminal completely complied with Lipinski's Rule of Five, which indicates high oral bioavailability. Compounds with several Lipinski violations, such as Tambuletin, were deemed less appropriate for oral administration because of the possibility of poor permeability or absorption. Since their advantageous pharmacokinetic characteristics increase the likelihood of a successful medication development process, substances with zero or few violations were given priority. This criterion was crucial in reducing the number of potential candidates for additional molecular docking and pharmacokinetics prediction.

Prediction of the toxic potential of possible drug candidates is one of the most crucial elements in contemporary drug discovery. The toxicity analysis revealed that the LD50 values of the studied compounds ranged from 3 mg/kg (class 4 toxicity) to 70000 mg/kg (class 6 toxicity) (Ruiz et al., 2012). The  $\alpha$ -Amyrins showed the highest LD50 value that indicated its low toxicity potential; however, it is proven highly immunotoxic. Cuminal, Sabinene and Phellandral showed nontoxic or mildly toxic effects whereas sulfadoxine exhibited slightly carcinogenic potential prompting serious safety concerns that resulted in its removal from further consideration. Following this toxicity assessment, only compounds categorized as non-toxic or mildly toxic were selected, culminating in the identification of 21 compounds for advanced molecular docking studies.

The results of molecular docking analysis revealed the strong binding of Pf AMA-1 (1Z40) with Cuminal (-5.9kcal/mol), Pf GST(1OKT) with Sabinene (-7.1 kcal/mol), and Pf DHFR with Phellandral (-5.5 kcal/mol). In addition to the binding energy, the interacting amino acid residues of the target protein and the hydrogen bond energy play an important role in determining the effect of selected ligand on the protein target. Cuminal has been investigated to interact with 3 amino acid residues of the malarial antigen PfAMA-1, Sabinene to interact with 6 amino acid residues of Pf GST, and Phellandral interacts with 3 amino acids of the Pf DHFR which shows increased specificity and stability of molecular structures. The standard drug, sulfadoxine, did not demonstrate an interaction with Pf AMA-1 (1Z40) and Pf GST (1OKT) (Tables 4, 5 and 6) (Jha et al., 2010). Cuminal exhibits strong affinity and stability through interactions involving hydrogen bonding, Pi-alkyl, and Pi-anion, reinforcing its potential for further drug development. The numerous

hydrogen bonds of sabinene suggest favorable binding alignment and the possibility of significant inhibitory effects. The mixed bonding types of Phellandral indicate a level of moderate stability and specificity at the active site. Although sulfadoxine did not demonstrate significant binding to PfAMA-1 or PfGST in our docking study, it was used as a reference drug due to its established clinical use against *P. falciparum*. This further confirms the accuracy of the docking conducted in your research. The main target is dihydropteroate synthase (DHPS), involved in the folate synthesis pathway, rather than the proteins investigated in this study. Consequently, the lack of significant interactions with AMA-1 or GST does not undermine its role as a comparator; instead, it emphasizes the uniqueness of our target-based methodology. Artesunate, exhibiting robust binding affinities with all three targets and varied interactions, acts as a positive control, verifying that the proteins you selected are appropriate and that the docking approach effectively identifies significant interactions. In summary, these findings advocate for the potential repositioning or development of Cuminal, Sabinene, and Phellandral as innovative inhibitors, while underscoring the importance of multi-target binding in improving antimalarial effectiveness and decreasing the risk of resistance.

Molecular dynamics simulation studies are frequently used as a rational approach in predictive studies of potential ligand–receptor interactions to aid the process of drug design and development (Salmaso and Moro, 2018). A molecular dynamics simulation via GROMACS was performed and the RMSF, RMSD, and Rg values were measured to assess the stability and flexibility of docked complexes such as Cuminal and PfAMA-1, Sabinene and PfGST, and Phellandral and PfDHFR. All the three ligands showed small deviations in the binding energies which reveals the stable interactions. Sabinene shows the lowest deviations, suggesting a very strong and stable interaction, while the RMSD analysis validate structural consistency across all complexes. Phellandral notably causes a little compaction, which may contribute to increased structural rigidity, according to the Radius of Gyration (Rg) profiles, which indicate that ligand binding is not affecting the protein's overall folding. Likewise, the decreasing SASA for Phellandral suggests a tighter packing and less flexibility, whereas the constant SASA values for Cuminal and Sabinene show sustained solvent exposure. The RMSF data further show that, as a result of ligand-induced stability of key residues, fluctuations are mostly limited to the terminal and loop regions, with little movement seen near the active sites. These results collectively imply that all three ligands preserve the structural integrity of 3 proteins while producing complexes that are dynamically stable and energetically favorable, supporting their possible function in blocking parasite detoxification processes.

The main objective of this research was to create and evaluate potential compounds derived from *Z. armatum* that could imitate or enhance the therapeutic mechanisms of artemisinin, potentially aiming for the same pathways or producing multi-target effects. The isolated compounds from *Z. armatum* were assessed based

on their anticipated binding affinities, their ability to produce reactive oxygen species, and their interaction with crucial proteins involved in parasite metabolism and survival. These identified compounds might work similarly to artemisinin by inducing oxidative stress in the parasite or complement artemisinin by targeting other essential pathways for the parasite's survival, thus creating a synergistic effect in combined therapies (Omari et al., 2021).

One of the phytochemicals proven to be effective in our study was Cuminal. It is also known as Cuminaldehyde (CA) that regulates the formation of genes involved in synaptic plasticity and neurotrophic factors and thus modulates the process of memory and learning and causes neuroprotective effects (Omari et al., 2021). CA (25–100 mg/kg) helps to reduce inflammation by decreasing the serum concentration of IL-1 $\beta$  and TNF- $\alpha$  in chronic constriction injury (CCI)-induced neuropathy (Koohsari et al., 2020). Recently, it has been implicated in the treatment of diabetes by affecting insulin levels, however, further research is warranted to identify its role in diabetes and other disorders such as malaria (Duraismy et al., 2022).

Another important bioactive compound that has been shown to be effective against malaria in our study is Sabinene, which is known to reduce muscle atrophy by affecting the ROS-facilitated MAPK/MuRF-1 signaling pathway (Ryu et al., 2019). Sabinene treatment also decreased reactive oxygen species (ROS) and attenuated the levels of different antioxidant enzymes such as lipid peroxidase, GST and catalase in yeast cells (Sharma et al., 2019). As plasmodial GST is an important target of antimalarial drugs and in our study Sabinene also showed a stable interaction with Pf GST, so it may act as a promising agent for the treatment of malaria, however, further *in vivo* and clinical studies are required to validate its role in the treatment of malaria.

In the same study, exposure to Sabinene prevented the angiogenesis (Sharma et al., 2019). As angiogenesis is an important hallmark of cancer, it is postulated that Sabinene may cause beneficial effects in preventing cancer by inhibiting angiogenesis.

The essential oil of *Eucalyptus camaldulensis* is known to possess Phellandral and Cuminal in reasonable concentrations (1.4–4.7%) and this oil has been shown to be beneficial in preventing the growth of phytopathogenic fungi, so it is possible that Phellandral may act as an antifungal agent (Barra et al., 2010). Our results showed the inhibitory potential of Phellandral against Pf DHFR; however, the literature is scarce regarding the role of this very compound in disease treatment and prevention; therefore, it may serve as a novel research target for the management of malaria and other pathogenic conditions.

These phytochemicals target various important proteins that play a crucial role in malaria and these proteins are identified via network pharmacology method. The identified proteins are required for the normal functioning of the malarial parasite. According to the network pharmacology approach, Cuminal target proteins involve ALB, PTPRC, CXCL8, NOS2, HMOX1, MPO, and GSR, Sabinene targets for the



Sabinene include MPO, TNF, IDO1, and NOS2, whereas Phellandral mainly through MPO, IL6, PTPRC and NOS2. All compounds target nitric oxide synthase (NOS2) and myeloperoxidase (MPO). NOS2 modulated nitric oxide (NO) and NO helps fight against malarial parasite (Levesque et al., 2010) by producing oxidative stress and inhibiting its growth, and it also activates the immune system to produce pro-inflammatory cytokines and clear the parasite. However, increased production of NO can cause damaging effects in the host and cause ROS production, leading to oxidative stress and inflammation in the host; therefore, an intricate balance in NO production of NO is required to combat pathogens (Kotepui et al., 2023). The phytochemicals selected in this study can prevent the NOS2 thus regulating the production of NO in the event of malaria.

MPO is mainly produced by monocytes and is neutrophils and involved in ROS production; however, its exact role in malaria is still unknown. Increased levels of MPO are observed in malarial patients with increased parasitemia, and regional/altitudinal differences were observed between Santa, Bambili, and Bamenda (Ngum et al., 2023).

## CONCLUSION

The present study explored the therapeutic potential of 40 natural bioactive compounds of *Z. armatum* against the *P. falciparum*. Molecular docking showed the stable complexes of three phytoconstituents such as Cuminal, Sabinene, and Phellandral against PfAMA-1, Pf GST, and Pf DHFR, respectively, which reveals their potential in mitigating malaria. Molecular dynamic simulations and network pharmacology analysis further confirmed the role of Cuminal, Sabinene, and Phellandral in inhibiting antigen and enzymes crucial for the pathogenesis of *P. falciparum*. Our study provides a strong basis for further *in vitro* and *in vivo* experimentation to validate the potential of these bioactive compounds in the treatment of malaria alone or in combination with available treatment options.

## REFERENCES

- Ahmad, A., Misra, L. N., and Gupta, M. M. 1993. Hydroxyalk-(4Z)-enoic acids and volatile components from the seeds of *Zanthoxylum armatum*. *Journal of Natural Products* 56(4), 456-460.
- Aminake, M. N., Mahajan, A., Kumar, V., Hans, R., Wiesner, L., Taylor, D., de Kock, C., Grobler, A., Smith, P. J., and Kirschner, M. 2012. Synthesis and evaluation of hybrid drugs for a potential HIV/AIDS-malaria combination therapy. *Bioorganic and Medicinal Chemistry*, 20(16), 5277–5289. <https://doi.org/10.1016/j.bmc.2012.06.045>
- Arunkumar, S., Ramalakshmi, N., Banu Priya, S., Hemalatha, B., Mani Megalai, P., Padma, K., and Jayashree, S. (2018). In silico design, docking, and synthesis of 3-hydroxy-3-methylglutaryl-coenzyme A reductase inhibitors. *Drug Invention Today*, 10(1), 1–5.
- Barra, A., Coroneo, V., Dessi, S., Cabras, P., and Angioni, A. 2010. Chemical variability, antifungal and antioxidant activity of *Eucalyptus camaldulensis* essential oil from Sardinia. *Natural Product Communications*, 5(2), 329–335. <https://doi.org/10.1177/1934578X1000500232SCIRP+1SCIRP+1>
- Barile, F. A. 1996. Drug toxicity assessment. En *In vitro* methods in pharmaceutical research (pp. 33–50). Academic Press.
- Banerjee, P., Eckert, A. O., Schrey, A. K., and Preissner, R. 2018. ProTox-II: A webserver for the prediction of toxicity of chemicals. *Nucleic Acids Research*, 46(W1), W257–W263. <https://doi.org/10.1093/nar/gky318>

- Basu, S., and Sahi, P. K. 2017. Malaria: An update. *The Indian Journal of Pediatrics*, 84(7), 521–528. <https://doi.org/10.1007/s12098-017-2332-2>
- Barkatullah, M. I., Jelani, G., and Ahmad, I. 2014. Leaf, stem bark and fruit anatomy of *Zanthoxylum armatum* DC. (Rutaceae). *Pakistan Journal of Botany*, 46(4), 1343–1349.
- Citaristi, I. (2022). World Health Organization—WHO. En *The Europa Directory of International Organizations 2022* (pp. 380–395). Routledge. <https://doi.org/10.4324/9781003292548-79>
- Daxon, B. 2019. Severe perioperative hypoxemic respiratory failure. En *A48. Critical Care Case Reports: Causes and Complications of Acute Respiratory Failure*. American Thoracic Society. <https://www.atsjournals.org/doi/book/10.1164/ajrcem-conference.2019.A48atsjournals.org>
- Duraisamy, K., Leelavinothan, P., Ellappan, P., Balaji, T. D. S., Rajagopal, P., Jayaraman, S., and Babu, S. 2022. Cuminaldehyde ameliorates hyperglycemia in diabetic mice. *Frontiers in Bioscience-Elite*, 14(4), 24. <https://doi.org/10.31083/j.fbe1404024ResearchGate+1PubMed+1>
- Dhami, A., Palariya, D., Singh, A., Kumar, R., Prakash, O., Kumar, R., and Pant, A. 2018. Chemical composition, antioxidant, *in vitro* anti-inflammatory and antibacterial activity of seeds essential oil of *Zanthoxylum armatum* DC. Collected from two different altitudes of Kumaun region, Uttarakhand. *Int. J. Chem. Stud.*, 6(6), 363–370.
- Eastman, R. T., and Fidock, D. A. 2009. Artemisinin-based combination therapies: A vital tool in efforts to eliminate malaria. *Nature Reviews Microbiology*, 7(12), 864–874. <https://doi.org/10.1038/nrmicro2239OUCI+1Nature+1>
- Fikadu, M., and Ashenafi, E. 2023. Malaria: An overview. *Infection and Drug Resistance*, 16, 3339–3347. <https://doi.org/10.2147/IDR.S408382>
- Francis, J. A., Shalauddin, M., Ridzwan, N. F. W., Mohamad, S. B., Basirun, W. J., and Tayyab, S. 2020. Interaction mechanism of an antimalarial drug, sulfadoxine with human serum albumin. *Spectroscopy Letters*, 53(5), 391–405.
- Greenwood, B. (1997). The epidemiology of malaria. *Annals of Tropical Medicine and Parasitology*, 91(7), 763–769. <https://doi.org/10.1080/00034983.1997.11813211PubMed>
- Guadie, M., Molla, E., Mekonnen, M., and Cerdà, A. 2020. Effects of soil bund and stone-faced soil bund on soil physicochemical properties and crop yield under rain-fed conditions of Northwest Ethiopia. *Land*, 9(1), 13. <https://doi.org/10.3390/land9010013>
- Hopkins, A. L. (2007). Network pharmacology. *Nature Biotechnology*, 25(10), 1110–1111. <https://doi.org/10.1038/nbt1007-1110PubMed+3discovery.dundee.ac.uk+3Nature+3>
- Huey, R., Morris, G. M., and Forli, S. 2012. Using AutoDock 4 and AutoDock Vina with AutoDockTools: A tutorial. The Scripps Research Institute Molecular Graphics Laboratory.
- Iqbal, I., and Hamayun, M. 2004. Studies on the traditional uses of plants of Malam Jabba valley, District Swat, Pakistan. *Ethnobotanical Leaflets*, 2004(1), 15.
- Jha, P. K., Sknepnek, R., Guerrero-García, G. I., and Olvera de la Cruz, M. 2010. A graphics processing unit implementation of Coulomb interaction in molecular dynamics. *Journal of Chemical Theory and Computation*, 6(10), 3058–3065. <https://doi.org/10.1021/ct100260z>
- Jindal, D., and Rani, V. 2023. In silico studies of phytoconstituents from *Piper longum* and *Ocimum sanctum* as ACE2 and TMRSS2 inhibitors: Strategies to combat COVID-19. *Applied Biochemistry and Biotechnology*, 195(6), 2618–2635. <https://doi.org/10.1007/s12010-022-04294-7>
- Kumari, R., Mishra, R. C., Yadav, S., and Yadav, J. P. 2019. Exploring molecular docking studies of alanine racemase inhibitors from *Elettaria cardamomum*. *Current Enzyme Inhibition*, 15(2), 91–102. <https://doi.org/10.2174/1573408015666190619120643OUCI>
- Khan, A., Rahman, M., and Islam, M. (2008). Antibacterial, antifungal and cytotoxic activities of amblyone isolated from *Amorphophallus campanulatus*. *Indian Journal of Pharmacology*, 40(1), 41–44. <https://doi.org/10.4103/0253-7613.40487>
- Khan, T., Dixit, S., Ahmad, R., Raza, S., Azad, I., Joshi, S., and Khan, A. R. (2017). Molecular docking, PASS analysis, bioactivity score prediction, synthesis, characterization and biological activity evaluation of a functionalized 2-butanone thiosemicarbazone ligand and its complexes. *Journal of Chemical Biology*, 10(3), 91–104. <https://doi.org/10.1007/s12154-017-0167-ySpringerLink>
- Koohsari, S., Sheikholeslami, M. A., Parvardeh, S., Ghafghazi, S., Samadi, S., Poul, Y. K., Pouriran, R., and Amiri, S. 2020. Antinociceptive and antineuropathic effects of Cuminaldehyde, the major constituent of *Cuminum cyminum* seeds: Possible mechanisms of action. *Journal of Ethnopharmacology*, 255, 112786. <https://doi.org/10.1016/j.jep.2020.112786>
- Khanal, P. (2021). Antimalarial and anticancer properties of artesunate and other artemisinins: current development. *Monatshefte für Chemie-Chemical Monthly*, 152, 387–400.
- Kotepui, K. U., Mahittikorn, A., Wilairatana, P., Masangkay, F. R., and Kotepui, M. 2023. Association between *Plasmodium* infection and nitric oxide levels: A systematic review and meta-analysis. *Antioxidants*, 12(10), 1868. <https://doi.org/10.3390/antiox12101868media.malariaworld.org+2MDPI+2tm.mahidol.ac.th+2>
- Kamaraj, C., Ragavendran, C., Prem, P., Naveen Kumar, S., Ali, A., Kazmi, A., Ullah, A., Chandra Satish Kumar, R., Khan, S. U., and Luna-Arias, J. P. 2023. Exploring the therapeutic potential of traditional antimalarial and antidengue plants: A mechanistic perspective. *Canadian Journal of Infectious Diseases and Medical Microbiology*, 2023, 1860084. <https://doi.org/10.1155/2023/1860084>

- Levesque, M. C., Hobbs, M. R., O'Loughlin, C. W., Chancellor, J. A., Chen, Y., Tkachuk, A. N., Booth, J., Patch, K. B., Allgood, S., Pole, A. R., Fernandez, C. A., Mwaikambo, E. D., Mutabingwa, T. K., Fried, M., Sorensen, B., Duffy, P. E., Granger, D. L., Anstey, N. M., and Weinberg, J. B. 2010. Malaria severity and human nitric oxide synthase type 2 (NOS2) promoter haplotypes. *Human Genetics*, 127(2), 163–182. <https://doi.org/10.1007/s00439-009-0753-3>
- Malami, I., Jagaba, N. M., Abubakar, I. B., Muhammad, A., Alhassan, A. M., Waziri, P. M., Yahaya, I. Z. Y., Mshelia, H. E., and Mathias, S. N. 2020. Integration of medicinal plants into the traditional system of medicine for the treatment of cancer in Sokoto State, Nigeria. *Heliyon*, 6(3), e03501. <https://doi.org/10.1016/j.heliyon.2020.e03501>
- Muhammed, D., Adebiyi, Y. H., Odey, B. O., Alawode, R. A., Lawal, A., Okunlola, B. M., Ibrahim, J., and Berinyuy, E. B. 2021. *Dennettia tripetala* (pepper fruit): A review of its ethno-medicinal use, phyto-constituents, and biological properties. *GSC Advanced Research and Reviews*, 6(3), 35–43. <https://doi.org/10.30574/gscarr.2021.6.3.0089>
- Muregi, F. W., Kirira, P. G., and Ishih, A. 2011. Novel rational drug design strategies with potential to revolutionize malaria chemotherapy. *Current Medicinal Chemistry*, 18(1), 113–143. <https://doi.org/10.2174/092986711793979742>
- Mukhtar, H. M., and Kalsi, V. 2018. A review on medicinal properties of *Zanthoxylum armatum* DC. *Research Journal of Pharmacy and Technology*, 11(5), 2131–2138. <https://doi.org/10.5958/0974-360X.2018.00395.5>
- Miller, L. H., Good, M. F., and Milon, G. 1994. Malaria pathogenesis. *Science*, 264(5167), 1878–1883. <https://doi.org/10.1126/science.8009217>
- Narwal, S., Dhanda, T., Sharma, P., Sharma, V., Dhankhar, S., Garg, N., Ghosh, N. S., and Rani, N. 2024. Current therapeutic strategies for Chagas disease. *Anti-Infective Agents*, 22(1), 20–30. <https://doi.org/10.2174/2211352519666221228120031>
- Najmi, A., Javed, S. A., Al Bratty, M., and Alhazmi, H. A. 2022. Modern approaches in the discovery and development of plant-based natural products and their analogues as potential therapeutic agents. *Molecules*, 27(1), 349. <https://doi.org/10.3390/molecules27010349>
- Ndombera, F., Maiyoh, G., and Tuei, V. 2019. Pharmacokinetic, physicochemical and medicinal properties of N-glycoside anti-cancer agent more potent than 2-deoxy-D-glucose in lung cancer cells. *Journal of Pharmacology and Experimental Therapeutics*, 370(3), 1–10
- Ngum, N. H., Fakeh, N. B., Lem, A. E., and Mahamat, O. 2023. Prevalence of malaria and associated clinical manifestations and myeloperoxidase amongst populations living in different altitudes of Mezam division, North West Region, Cameroon. *Malaria Journal*, 22, 20. <https://doi.org/10.1186/s12936-022-04438-6PMC+1>
- Obonyo, D. O. 2022. Antibody-mediated natural killer cell function against *Plasmodium falciparum* [Tesis doctoral, Open University (Reino Unido)].
- Ogony, J. O. 2021. Correlates and incidence of *Plasmodium falciparum* among HIV infected and HIV non-infected children below 5 years in Kisumu County, Kenya [Tesis de maestría, Jomo Kenyatta University of Agriculture and Technology].
- Omari, Z., Sasaki, K., Sabti, M., Bejaoui, M., Hafidi, A., Gadhi, C., and Isoda, H. 2021. Dietary administration of cumin-derived Cuminaldehyde induces neuroprotective and learning and memory enhancement effects in aging mice. *Aging (Albany NY)*, 13(2), 1671–1685. <https://doi.org/10.18632/aging.202516>
- Pan American Health Organization. 2017a. Epidemiological alert: Increase in cases of malaria. PAHO/WHO. <https://www.paho.org/hq/dmdocuments/2017/2017-feb-15-phe-epi-alert-malaria.pdf>
- Pan American Health Organization (PAH). 2017b. Epidemiological alert: Increase in cases of malaria. PAHO/WHO. <https://www.paho.org/hq/dmdocuments/2017/2017-feb-15-phe-epi-alert-malaria.pdf>
- Peana, A. T., D'Aquila, P. S., Panin, F., Serra, G., Pippia, P., and Moretti, M. D. L. 2002. Anti-inflammatory activity of linalool and linalyl acetate constituents of essential oils. *Phytomedicine*, 9(8), 721–726. <https://doi.org/10.1078/094471102321621322>
- Pollastri, M. P. 2010. Overview on the Rule of Five. *Current Protocols in Pharmacology*, 49, 9.12.1–9.12.18. <https://doi.org/10.1002/0471141755.ph0912s49>
- Pomaznoy, M., Ha, B., and Peters, B. 2018. GOnet: A tool for interactive Gene Ontology analysis. *BMC Bioinformatics*, 19, 470. <https://doi.org/10.1186/s12859-018-2533-3tools.dice-database.org+6PubMed+6ResearchGate+6>
- Phillips, R. E., and Pasvol, G. (1992). Anaemia of *Plasmodium falciparum* malaria. *Baillière's Clinical Haematology*, 5(2), 315–330. [https://doi.org/10.1016/S0950-3536\(11\)80022-3](https://doi.org/10.1016/S0950-3536(11)80022-3)
- Phuyal, N., Jha, P. K., Raturi, P. P., and Rajbhandary, S. 2019. *Zanthoxylum armatum* DC.: Current knowledge, gaps and opportunities in Nepal. *Journal of Ethnopharmacology*, 229, 326–341. <https://doi.org/10.1016/j.jep.2018.09.035>
- Prugnolle, F., Durand, P., Ollomo, B., Duval, L., Arieu, F., Arnathau, C., Gonzalez, J.-P., Leroy, E., and Renaud, F. 2011. A fresh look at the origin of *Plasmodium falciparum*, the most malignant malaria agent. *PLoS Pathogens*, 7(2), e1001283. <https://doi.org/10.1371/journal.ppat.1001283>
- Ram, S., More-Adate, P., Tagalpallewar, A. A., Pawar, A. T., Nagar, S., and Baheti, A. M. 2023. An *in-silico* investigation and network pharmacology-based approach to explore the anti-breast-cancer potential of *Tectaria coadunata* (Wall.) C. Chr. *Journal of Biomolecular Structure and Dynamics*, 1–12. <https://doi.org/10.1080/07391102.2023.2252091>
- Ruiz, P., Begliutti, G., Tincher, T., Wheeler, J., and Mumtaz, M. 2012. Prediction of acute mammalian toxicity using QSAR methods: A case study of sulfur mustard and its breakdown products. *Molecules*, 17(8), 8982–9001. <https://doi.org/10.3390/molecules17088982>

- Ryu, Y., Lee, D., Jung, S. H., Lee, K.-J., Jin, H., Kim, S. J., Lee, H. M., Kim, B., and Won, K.-J. 2019. Sabinene prevents skeletal muscle atrophy by inhibiting the MAPK–MuRF-1 pathway in rats. *International Journal of Molecular Sciences*, 20(19), 4955. <https://doi.org/10.3390/ijms20194955>
- Salmaso, V., and Moro, S. (2018). Bridging molecular docking to molecular dynamics in exploring ligand–protein recognition process: An overview. *Frontiers in Pharmacology*, 9, 923. <https://doi.org/10.3389/fphar.2018.00923>
- Singh, S. S., Gupta, A., and Verma, A. 2013. Molecular properties and bioactivity score of the *Aloe vera* antioxidant compounds—in order to lead finding. CAB Abstracts.
- Sharma, S., Sharma, A., and Gupta, U. 2021. Molecular docking studies on the anti-fungal activity of *Allium sativum* (garlic) against mucormycosis (black fungus) by BIOVIA Discovery Studio Visualizer 21.1.0.0. *Annals of Antivirals and Antiretrovirals*, 5(1), 28–32.
- Sharma, S., Gupta, J., Prabhakar, P. K., Gupta, P., Solanki, P., and Rajput, A. 2019. Phytochemical repurposing of natural molecule: Sabinene for identification of novel therapeutic benefits using in silico and *in vitro* approaches. *Assay and Drug Development Technologies*, 17(8), 339–351. <https://doi.org/10.1089/adt.2019.939>
- Shamshad, H., Bakri, R., and Mirza, A. Z. 2022. Dihydrofolate reductase, thymidylate synthase, and serine hydroxymethyltransferase: Successful targets against some infectious diseases. *Molecular Biology Reports*, 49(9), 6659–6691. <https://doi.org/10.1007/s11033-022-07768-3>
- Shah, S. S., Ahmed, S., Zhou, B., and Shi, L. 2024. A review on pharmacological activities and phytochemical constituents of *Zanthoxylum armatum* DC. *Natural Product Research*, 1–20.
- Tahita, M. C., Tinto, H., Menten, J., Ouedraogo, J.-B., Guiguemdé, R. T., van Geertruyden, J. P., Erhart, A., and D'Alessandro, U. 201. Clinical signs and symptoms cannot reliably predict *Plasmodium falciparum* malaria infection in pregnant women living in an area of high seasonal transmission. *Malaria Journal*, 12, 1–7. <https://doi.org/10.1186/1475-2875-12-164>
- Tabassum, S., Khalid, H. R., Haq, W. u., Aslam, S., Alshammari, A., Alharbi, M., Riaz Rajoka, M. S., Khurshid, M., and Ashfaq, U. A. 2022. Implementation of system pharmacology and molecular docking approaches to explore active compounds and mechanism of *Ocimum sanctum* against tuberculosis. *Processes*, 10(2), 298. <https://doi.org/10.3390/pr10020298MDPI>
- Tao, W., Xu, X., Wang, X., Li, B., Wang, Y., Li, Y., and Yang, L. 2013. Network pharmacology-based prediction of the active ingredients and potential targets of Chinese herbal Radix Curcumae formula for application to cardiovascular disease. *Journal of Ethnopharmacology*, 145(1), 1–10. <https://doi.org/10.1016/j.jep.2012.09.051>
- ter Kuile, F. O., van Eijk, A. M., and Filler, S. J. 2007. Effect of sulfadoxine-pyrimethamine resistance on the efficacy of intermittent preventive therapy for malaria control during pregnancy: A systematic review. *JAMA*, 297(23), 2603–2616. <https://doi.org/10.1001/jama.297.23.2603>
- Tiwary, M., Naik, S., Tewary, D. K., Mittal, P., and Yadav, S. 2007. Chemical composition and larvicidal activities of the essential oil of *Zanthoxylum armatum* DC (Rutaceae) against three mosquito vectors. *Journal of vector borne diseases*, 44(3), 198.
- van der Spoel, D., Lindahl, E., Hess, B., Groenhof, G., Mark, A. E., and Berendsen, H. J. C. 2005. GROMACS: Fast, flexible, and free. *Journal of Computational Chemistry*, 26(16), 1701–1718. <https://doi.org/10.1002/jcc.20291>
- Vong, A. D.-Y., Hwang, S.-S., Chee, X. W. Z., and Sim, E. U.-H. 2022. Computational ligand–receptor docking simulation of piperine with apoptosis-associated factors. *Journal of Applied Biology and Biotechnology*, 10(1), 38–44. <https://doi.org/10.7324/JABB.2021.100105>
- Wang, J., Uddin, M. N., Wang, R., Gong, Y.-H., and Wu, Y. 2022. Comprehensive analysis and validation of novel immune and vascular remodeling related genes signature associated with drug interactions in pulmonary arterial hypertension. *Frontiers in Genetics*, 13, 922213. <https://doi.org/10.3389/fgene.2022.922213>
- Wang, S., Wu, R., Lu, J., Jiang, Y., Huang, T., and Cai, Y. D. 2022. Protein–protein interaction networks as miners of biological discovery. *Proteomics*, 22(15–16), e2100190. <https://doi.org/10.1002/pmic.202100190>
- Warrell, D. A., Watkins, W. M., and Winstanley, P. A. 2017. Treatment and prevention of malaria. En *Essential Malariology* (4<sup>th</sup> ed., pp. 268–312). CRC Press.
- Zoete, V., Cuendet, M. A., Grosdidier, A., and Michielin, O. 2011. SwissParam: A fast force field generation tool for small organic molecules. *Journal of Computational Chemistry*, 32(11), 2359–2368. <https://doi.org/10.1002/jcc.21816>
- Zhou, T., Yao, J., and Liu, Z. 2017. Gene ontology, enrichment analysis, and pathway analysis. En Z. Liu (Ed.), *Bioinformatics in aquaculture: Principles and methods* (pp. 150–168). Wiley-Blackwell. <https://doi.org/10.1002/9781118782392>